A Probabilistic Framework for the Fatigue Damage Assessment of Ships Navigating through Level Ice Fields

Weidong Zhao[1,2], Bernt Johan Leira[2], Ekaterina Kim[2], Guoqing Feng[1], Chana Sinsabvarodom[2]

1. Department of Shipbuilding Engineering, Harbin Engineering University, China

2. Department of Marine Technology, Norwegian University of Science and Technology, Norway

E-mail addresses:

zwd_ship@hrbeu.edu.cn (Weidong Zhao), bernt.leira@ntnu.no (Bernt Johan Leira), ekaterina.kim@ntnu.no (Ekaterina Kim), fengguoqing@hrbeu.edu.cn (Guoqing Feng),

chana.sinsabvarodom@ntnu.no (Chana Sinsabvarodom).

Highlights

1) A fatigue damage analysis procedure based on the application of numerical simulation tools is proposed for ships advancing in level ice fields.
2) The applicability of the procedure is illustrated using a hypothetical scenario with the Xuelong 2 icebreaker
3) The results show that the fatigue damage predicted by the proposed procedure is sensitive to boundary conditions, ship properties, and S-N curves.

Abstract

For ships navigating in ice-covered waters, fatigue damage due to ice loads is an important issue. The purpose of this paper is to provide ship researchers and engineers with a simulation-based procedure for a probabilistic fatigue damage assessment of ships moving through a level ice field. A novel procedure for fatigue damage assessment using numerical simulations is developed, and a hypothetical scenario with the *Xuelong 2* icebreaker is used to illustrate the procedure. Long-duration time-domain simulations are performed to generate samples of the ice-load peaks due to ship-ice interactions. Based on the average conditional exceedance rate (ACER) method, the extreme value statistics of the line load peaks are predicted, and subsequently, the fatigue stresses caused by ice loads are estimated by means of beam theory. Several analytical models are applied to describe the probability distribution of the stress amplitudes, and the fatigue damage is calculated based on S-N curves and the Palmgren-Miner formula. Furthermore, a quantification of the effects of uncertainties related to discretization errors (mesh size, reference period), ship-model properties, choice of boundary conditions, and S-N curves is performed.

Keywords: fatigue damage, level ice, ship-ice interaction, long-duration time domain, probabilistic method.

1 Introduction

The melting of ice in the Arctic, combined with the ever-increasing demand for

resources as well as the continuous advancement of modern technology, has promoted a growing interest in the Arctic region among many nations around the world. Increased activities in the Arctic regions promote further development of the requirements for the design and operation of ice-going vessels and offshore structures [1]. One concern is that vessels navigating through ice-covered waters are subjected to fatigue damage due to repeated ice actions. There is a need to develop new approaches to predict the reliability and useful life of ice-going vessels. This field of predictive modeling still faces many challenges, although extensive progress has been made in recent years [2-7].

Researchers have proposed many different approaches for the fatigue damage assessment of ships navigating in ice fields. The applied methods comprise in situ tests, fatigue analysis procedures and numerical simulations.

In terms of in situ tests, Chai and Leira [2] examined the short-term extreme value statistics of ice loads acting on a ship hull and considered fatigue damage due to ice loads. Furthermore, the relevance of various probabilistic models, such as the Weibull distribution and the exponential distribution, was studied. The application of a fatigue damage estimation procedure based on the corresponding probability density functions of the stress ranges was also illustrated. An and Lee [3] analyzed the fatigue damage index and fatigue life for the vessel ARAON based on its voyage schedules and the assumed routes of corresponding Antarctic voyages. Data records measured during Arctic transits in 2010 were utilized. However, studies of this type based on in-situ tests are generally associated with high costs and significant time resources.

As a part of a fatigue analysis procedure, the accumulated damage is predicted based on empirical or semiempirical methods [4-6]. Lloyd's Register [4] announced the ShipRight FDA ICE, a fatigue design evaluation procedure used to quantify the damage in hull structures subjected to ice loads. However, since the procedure contains many assumptions, the accuracy of the results can be strongly affected if these assumptions are invalidated. Suyuthi and Leira [5] proposed a systematic procedure for fatigue damage assessment in relation to ships navigating in ice-covered waters. Their procedure considered the variation in ice conditions, vessel speed, and operational modes. Some practical concerns related to the application of the proposed procedure were also discussed. However, since the main parameters for fatigue analysis were obtained from field measurement data, the application of this procedure to different conditions requires that a certain amount of corresponding case-specific data is available.

Currently, there are few approaches for probabilistic fatigue damage assessment based on numerical simulations of ship-ice interactions. Earlier works were frequently based on full-scale measurements and/or empirical and semiempirical equations. However, numerical simulations may offer extra advantages. As an example, numerical simulations are possible even with limited computational efforts, and a range of various ice conditions can easily be implemented [7].

The relevant literature shows that available methods for the fatigue assessment of ice-going ships are mainly based on two components: the generation of ice load

records and the application of a fatigue analysis procedure. Based on these factors, two aspects are important with respect to the probabilistic assessment of fatigue damage for ice-going vessels. The first is the ability to appropriately generate ice load records for various representative ice conditions and thermal states (e.g., level ice fields, broken ice fields, deformed ice fields). Second, an appropriate fatigue damage analysis method is required. This should also be accompanied by an uncertainty modeling technique to account for the stochastic nature of the fatigue process.

Fatigue is a long-term damage accumulation process caused by cyclic loading [8]. Ice load records simulated by transient analysis are usually a few seconds in duration, which accordingly is not adequate for the analysis of fatigue damage. It is thus important to obtain long-duration time-domain ice loads for the purpose of fatigue damage analysis. However, the generation of long-duration time histories by means of simulations can be extremely demanding for conventional numerical methods due to the significant cost and time resources involved. Kim [7] carried out fatigue damage assessments for an ice-going ship navigating through broken ice fields based on an application of the computer program ABAQUS. The ice-structure interaction (localized ice edge cruising) was modeled as a pressure-penetration curve with a direct proportionality between pressure and penetration. Accordingly, flexural failure was not accounted for in this model, thus making the procedure unsuitable for addressing fatigue damage in level ice. There is a need for simulation procedures that can consider different ice failure modes for the purpose of generating long-duration ice-load records, which are required for fatigue damage assessments.

This paper proposes a procedure for the assessment of fatigue damage due to ice loads using numerical simulations to generate ice load records. To illustrate the proposed procedure, a numerical example is provided. In this example, we have focused solely on the primary ice impact loads (ice crushing and flexural failure); however, the procedure itself is not limited to this consideration. To shed light on the effects of some of the assumptions introduced to simplify the probabilistic assessment, a numerical example in relation to the icebreaker Xuelong 2 is presented. We have studied sources of the uncertainties (i.e., boundary conditions, ship-model properties, S-N curves (normal temperature versus low temperature), mesh size, and reference period) and present the results of the analysis.

This paper can be outlined is as follows: Section 2 describes the proposed procedure. Section 3 presents an application example for the proposed procedure and an uncertainty quantification for the proposed approach. Section 4 discusses the effects of boundary conditions in relation to the fatigue point and the effects of applying a low-temperature S-N curve on the fatigue damage. The last section summarizes the primary conclusions drawn from the present study.

2 Proposed procedure

This section presents a new procedure for the probabilistic assessment of fatigue damage in ships navigating through level ice fields (see Fig. 1). Numerical simulations of ship-ice interaction are used in the proposed procedure as a tool to reconstruct the ice load signal and analyze the related fatigue damage. The procedure requires an ice model (constitutive equations, including fractures) and an ice-ship interaction model

(discretized geometry of the ice field and the ship structure, a water model, and a ship-water-ice contact model). The ship structure can be modeled as a rigid body or a deformable body. If a rigid body assumption is used, then the stress response can be predicted based on beam theory as described in Section 2.2.

In addition, a verification of the ice model and the ice-ship interaction algorithm should be performed. A long-period analysis model is capable of generating long sequences of time-domain simulations of the ship-ice interaction process, and the details of the long-period analysis can be found in Section 2.1.
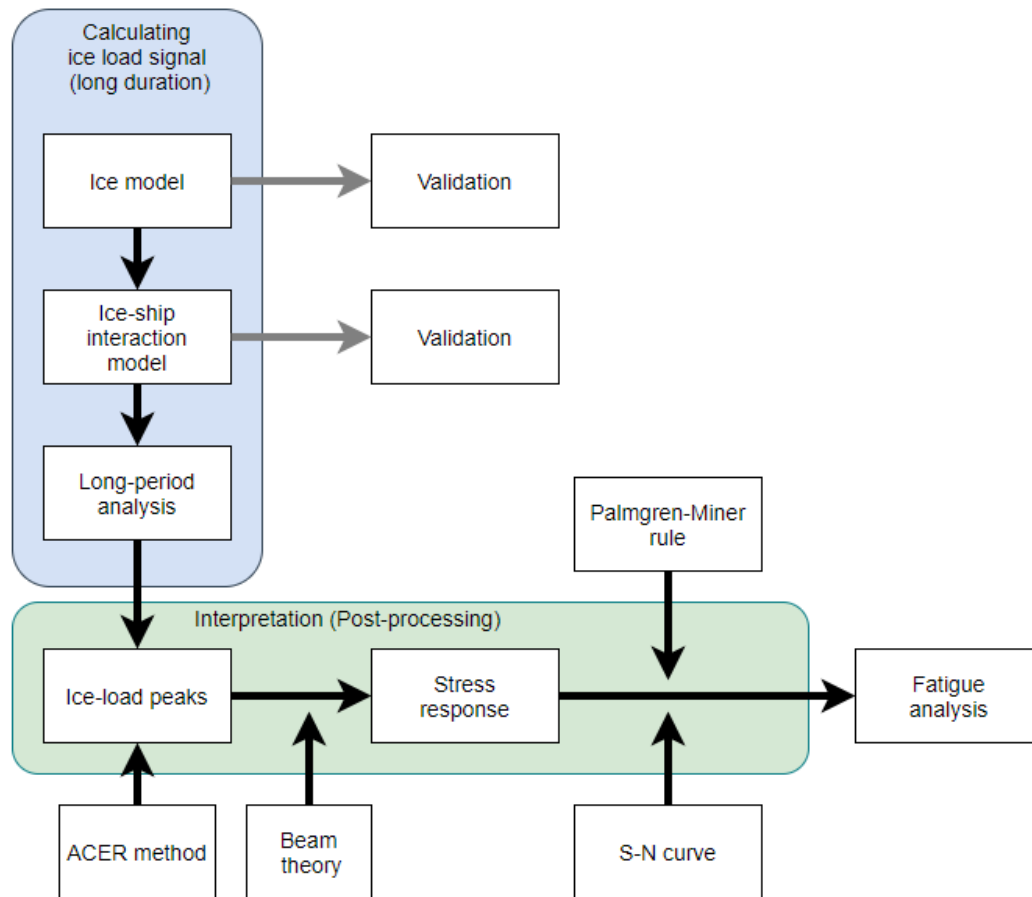
Fig. 1 The proposed procedure for ice-induced fatigue analysis

The generated ice load signal also needs to be postprocessed. First, extreme value statistics for the line load peaks are estimated based on the average conditional exceedance rate (ACER) method, and the line load peaks are converted into structural stresses at the relevant fatigue point by means of beam theory. Next, probabilistic models, such as the Weibull distribution, the lognormal distribution and the Gumbel distribution, are applied to approximate the distribution of the stress amplitudes due to ice load actions. Finally, the performance of the fatigue damage evaluation based on S-N curves and probabilistic distribution functions of the stress amplitudes is studied.

The proposed procedure can be used for other ice fields (e.g., ridged ice fields, broken ice fields, brash ice) by changing ice modeling techniques, ice-ship interaction

4

models, assumptions underlying reconstruction of the ice load signal, etc. The following paragraphs detail elements of the proposed procedure for long-duration simulations and interpretations of the ice load records for the purpose of fatigue analysis.

2.1 Analysis methodology for long-duration simulation in level ice

As a technique for long-duration simulations, we propose dividing ship-ice interactions into many subcases, which include ships, parts of level ice and water, as shown in Fig. 2. For each case N, the preload from the previous step of the analysis (N-1) is used as an input. When the finite element method is deployed as a solver of partial differential equations, the input to case N constitutes the prescribed deformation, shell thickness, and element history variables (stress, plastic strain, etc.).
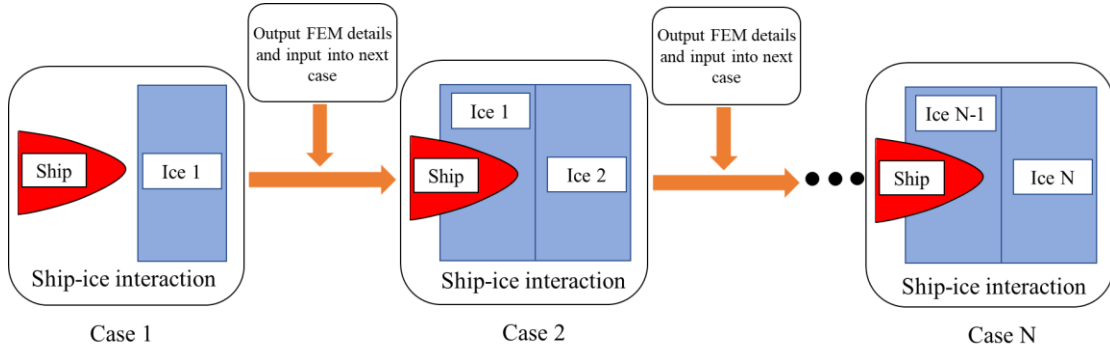
Fig. 2 The analysis methodology

This approach also requires a new level-ice geometry (Ice N) to be attached to the previous geometry (Ice N-1), and there should be common elements between the junction of the two level ice sheets. It is worth noting that the interaction between the adjacent level ice sheets can be considered by importing the stresses and displacements of the level ice from case N-1 to the ice sheet in case N as the initial stress and displacement conditions. In other words, for case N, the level ice in front of the ship is disturbed by the ship, and the adjacent level ice is disturbed from case N-1. Therefore, the ice loads are not repeated even though the same ice blocks continue to repeat.

2.2 Load-time history postprocessing for fatigue analysis

2.2.1 Extreme value statistics of ice loads

The local ice loads at n points can be obtained based on the local contact pressure between the hull and ice at the corresponding n points, for example, as shown in Fig. 3 (for $n=6$ points). Subsequently, the local ice loads are converted to line loads (kN/m) by dividing the local ice loads by the frame spacing; see, e.g., [9] and Figs. 4 (a) and (b).
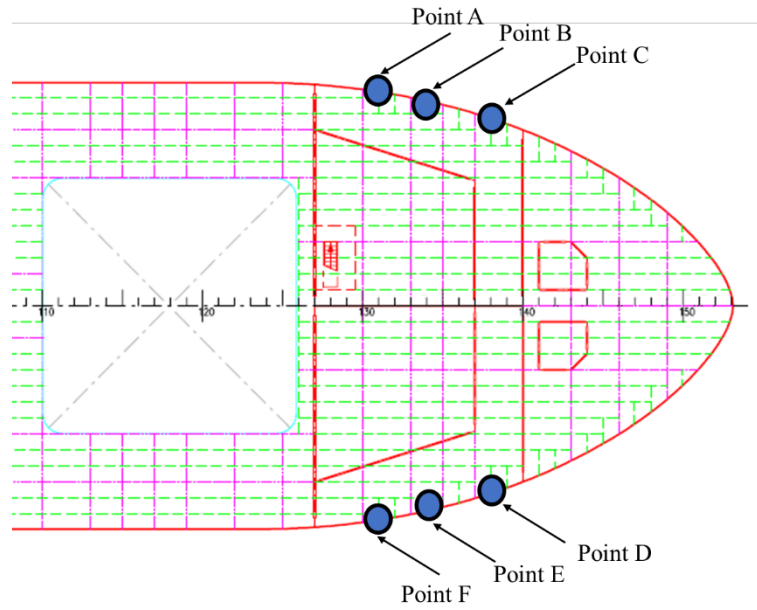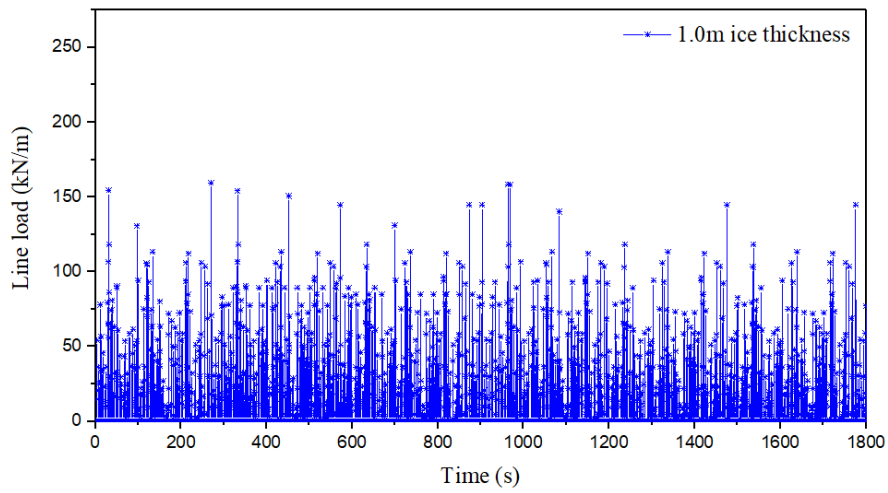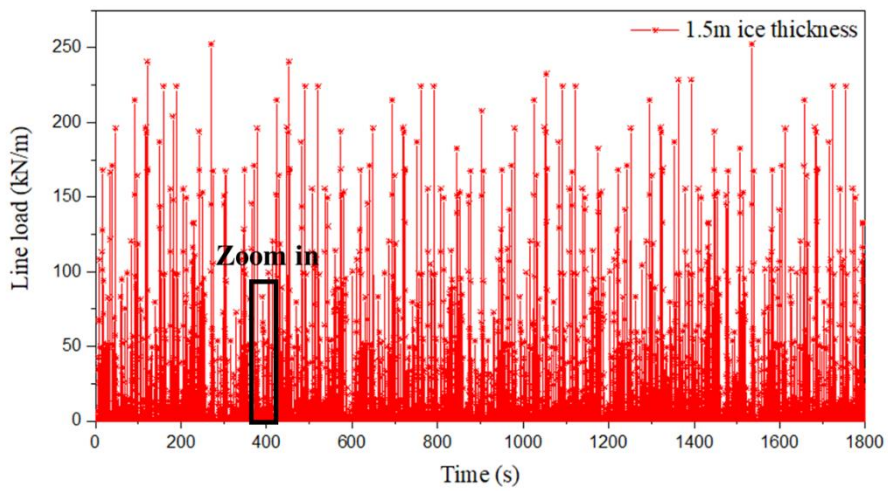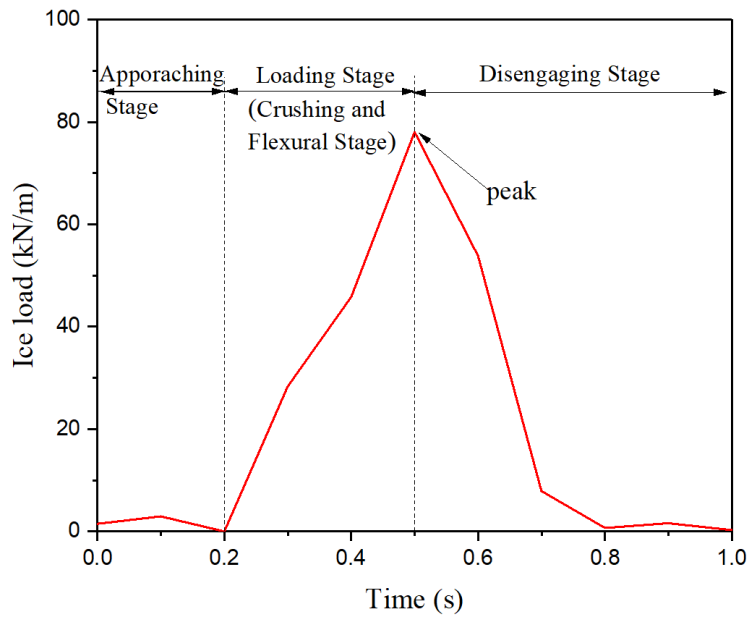
Fig. 3 Locations for monitoring points ($n=6$)

(a) Simulated line load corresponding to 1.0-m thick ice

(b) Simulated line load corresponding to 1.5-m thick ice

(c) A typical profile of a load impulse with distinct stages is shown in Fig. 4(b). Each impulse can be divided into 3 stages: (i) the approaching stage, (ii) the crushing and bending stage, and (iii) the disengaging stage as done in [10] by adding flexural failure.

Fig. 4 Time histories of line loads acting on the rigid ship hull (at point C)

The ice load cycles (or stress ranges) can be replaced by the ice load amplitudes, and the total number of ice load cycles is equal to the number of line load peaks [11]. The peaks are identified based on a predefined minimum peak distance; see, for example, Fig. 5.
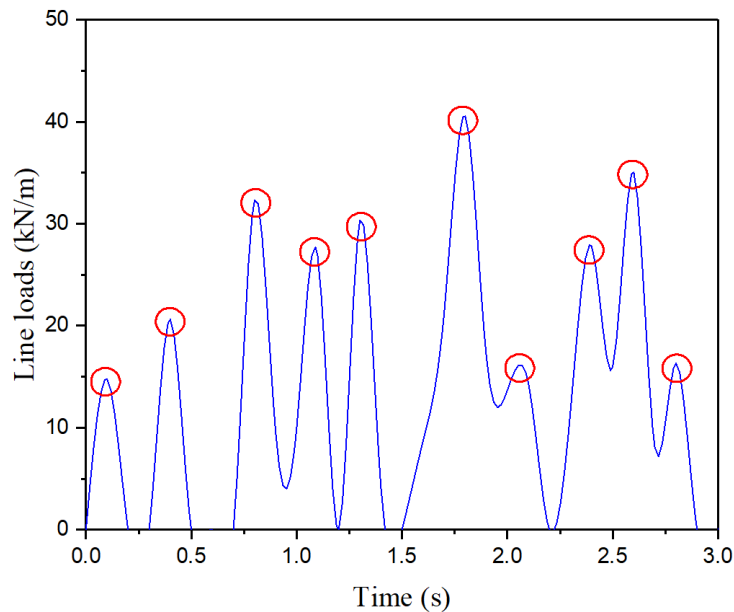

Fig. 5 Identification of line load peaks extracted by the "findpeaks" function in

Then, the statistics of extracted line load peaks need to be analyzed. At this stage, we propose to use the average conditional exceedance rate (ACER) method (Gaidai and Naess [13]) for estimation of the extreme ice load values, as was also used by Chai et al. [2]. In this method, a sequence of nonparametric functions, i.e., the ACER functions of different orders, are estimated and applied for the purpose of approximating the exact extreme value distribution.

Based on the simulated time series of line load peaks, the approximated distribution for the extreme values can be obtained using Eq. (1) (Gaidai and Naess [13]

$$\text{Prob}(M_N \leq \eta) \approx P_k(\eta) \approx \exp(-(N-k+1)\varepsilon(\eta)) \tag{1}$$

where

$M_N = \max\{X_1,\ldots,X_N\}$, $X_1,\ldots,X_N$ are the peak values (kN/m),

$\varepsilon_k(\eta)$ is the empirical ACER function of order k, which can be obtained by applying the available time series. $\varepsilon_k(\eta)$ is assumed to be in the form of:

$$\varepsilon_k(\eta) \approx q_k \exp(-a_k(\eta-b_k)^{c_k}), \eta \geq \eta_0 \tag{2}$$

where a_k, b_k, c_k and c_k are suitable constants that are dependent on the number of orders k. Other details of this method are provided by Naess and Gaidai [14].

2.2.2 Fatigue stress response calculations

In the case of a rigid ship structure, the dynamic stress response of structures can be calculated by structural beam theory or structural analysis [15] using the line load peaks (Section 2.2.1) as input. It is assumed here that there is a linear transformation between the local ice load process and the ice-induced stress response, and the transformation can be written as in [5]:

$$S(t) = \gamma X(t) \tag{3}$$

where

$X(t)$ is the line load peaks (kN/m) from Section 2.2.1,

$S(t)$ is the corresponding stress (MPa),

γ is the transformation factor.

To determine the value of γ in Eq. (3), the location and structural details of the fatigue points must first be determined. Lloyd's Register notes that the critical locations to be considered for fatigue due to ice loads are the end connections of frames and stiffeners of the side shell in the ice belt region of the ship [4]. The China Classification

Society has also issued similar guidelines [16].

For the fatigue point selected, the transformation factor γ can be determined by Eq. (4) and Eq. (5) [5].

$$\gamma = \frac{c_p l}{m_t Z} \times 10^3 \qquad (4)$$

and

$$m_t = \frac{7 m_0}{7 - 5h/l} \qquad (5)$$

where

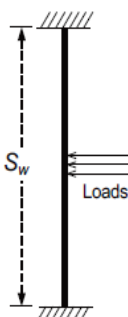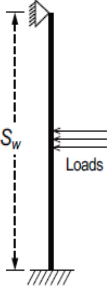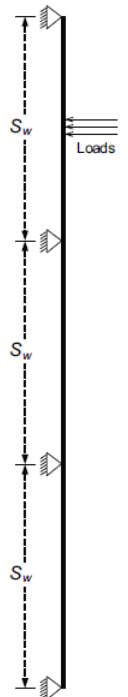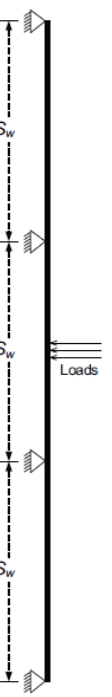l is the vertical span of the frame (m),

h is the height of the load area (m),

Z is the section modulus (cm^3), and

$c_p = s$, where s is the frame spacing (m) and

m_0 depends on the boundary conditions for the transverse frame, which can be determined based on Table 1 below [4].

Table 1 The boundary coefficients m_0 for transverse framing systems

Boundary Conditions			
a	b	c	d
m_0=8	m_0=5.3	m_0=10.0	m_0=13.3

2.2.3 Fatigue damage prediction method

The fatigue damage at the selected point in the hull of the icebreaker during a stationary short-term condition can be evaluated by applying the linear Palmgren-Miner equation, which is given by the following expression:

$$D = \sum_{i=1}^{w} \frac{n_i}{N_i} \qquad (6)$$

where

D is the fatigue damage accumulated during the stationary short-term condition,

n_i is the number of stress cycles for the stress range S_i, and

N_i is the number of stress cycles to failure for the stress range S_i, which is given by the S-N curve:

$$N_i = C \cdot S_i^{-m} \qquad (7)$$

in which C and m are intrinsic to the S-N curve that has been selected.

By combining Eq. (6) and Eq. (7), the fatigue damage can be calculated based on Eq. (8):

$$D = \frac{1}{C} \sum_{i=1}^{w} n_i S_i^m = \frac{N_t}{C} \sum_{i=1}^{w} S_i^m f_s(S_i) \Delta S \qquad (8)$$

Similarly, the fatigue damage based on a specific probability density model for the stress cycle range (i.e., S) can be written as:

$$D = \frac{N_t}{C} \int_0^\infty S^m f_s(S) \, \mathrm{d}S \qquad (9)$$

where

N_t is the total number of stress cycles during the simulation,

$f_s(S_i)$ is the point probability for stress range S_i,

$f_s(S)$ is the continuous probability density function of the stress ranges S, and

ΔS is the interval width of the stress ranges in the discretized formulation.

It is worth noting that the stress cannot be physically infinite. Hence, the upper limit of the integral in Eq. (9) is changed from infinite to a maximum stress S_{max}, as shown in Eq. (10):

$$D = \frac{N_t}{C} \int\limits_0^{S_{max}} S^m f_s(S)\, \mathrm{d}S \tag{10}$$

3 Application example: transit of the icebreaker Xuelong 2 in first-year sea ice

To illustrate the proposed procedure (Fig. 1), a numerical example is provided based on the finite element formulation and element deletion technique. The calculation of the ice load time history is performed with LS DYNA version R11.0 [17]. In this example, we have focused only on the primary ice impact loads due to ice crushing and flexural failure. However, the procedure itself is not limited to the above considerations.

For the purpose of fatigue damage assessment in level ice, no commonly accepted ice model exists. Thus, to illustrate the proposed approach, we selected a material model that can adequately represent ice crushing strength and ice flexural strength. This model is briefly described below, whereas details are given in the appendix.

3.1 Ice material model

The material class *MAT_PLASTICITY_COMPRESSION_TENSION (MAT 124) was chosen in LS DYNA, which is an isotropic elastic-plastic model [18]. The main reason for selecting this material model is its ability to model different behaviors in compression and tension. Moreover, it can also account for strain rate sensitivity. The same model was found to be most suitable (among LS-DYNA models) in representing forces during ship-ice interactions [19]. The representative material parameters for first-year sea ice at 0 °C are shown in Table 2. The values in Table 2 can be changed if the ice temperature changes.

Table 2 Parameters for the sea ice model [19-21]

Density, ρ	$900\,\mathrm{kg/m^3}$
Young modulus, E	9.45 GPa
Poisson's ratio, μ	0.3
Initial compressive strength, σ_c^0	5.8 MPa
Initial tensile strength, σ_t^0	0.58 MPa
Plastic hardening modulus, E_p	6 MPa
Effective plastic failure strain, ε_f	5E-5~5E-3
Compressive mean stress, σ_{mc}	$\sigma_c^0/3$
Tensile mean stress, σ_{mt}	$\sigma_t^0/3$

The equivalent plastic failure strain criterion is used in this analysis. When the equivalent plastic strain of an element reaches the defined critical value (ε_f), the element is deleted. The MAT_ADD_EROSION failure criterion used throughout this paper is the equivalent plastic failure strain. The ε_f value is adjusted to represent the proper compressive and flexural behavior of the ice as described in the following

subsections. Other details of sea ice material properties can be found in Appendix A.

3.2 Verification of the ice model

    As we have primarily focused on ice crushing and flexural failure, the ice material model performance is verified against the experimental data for uniaxial compression and bending tests. The results of the verification are reported in the following paragraphs, whereas the details of verification are given in Appendix A.
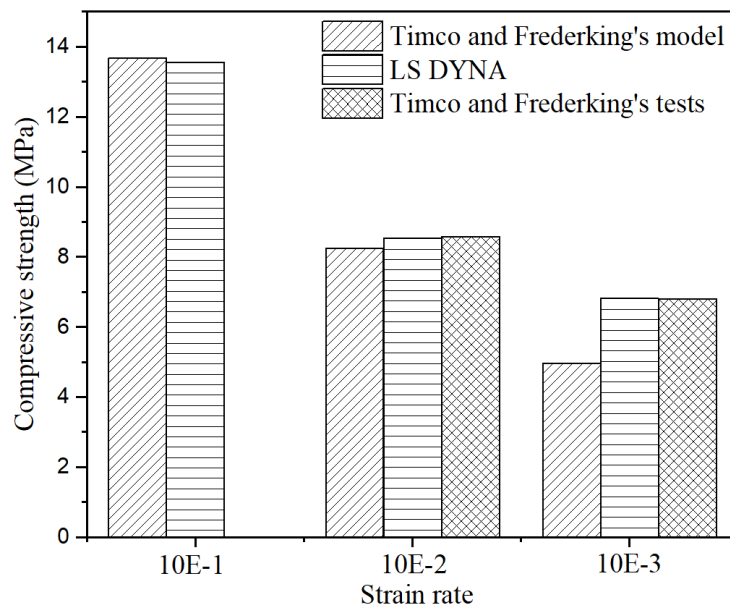

Fig. 6 The result for compressive loading. Timco and Frederking's model is from [22, 23], and Timco and Frederking's tests are the experimental data reported in [24].

    The results corresponding to compression at different strain rates are compared with the results of Timco and Frederking [24], as shown in Fig. 6. There is little difference among these results at 10E-2 s^{-1}; the results of Timco and Frederking's tests and LS DYNA are almost 2 MPa higher than those of Timco and Frederking's model at 10E-3 s^{-1}, while the result of LS DYNA is still consistent with that of Timco and Frederking's tests. For a strain rate of 10E-1 s^{-1}, there are no test results, but the analytical model and the LS DYNA results agree quite well. Generally, the material keywords MAT 124 and the applied ice material parameters are suitable for simulation of the behavior due to compressive loading for the purpose of illustrating the overall fatigue assessment procedure.
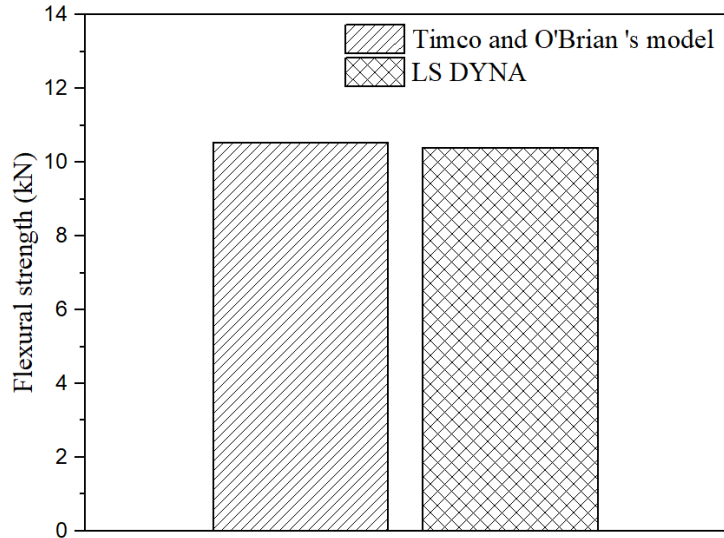
Fig. 7 Flexural strength of the ice beam

Fig. 7 provides a comparison between the flexural strength (10.4 kN) calculated by LS DYNA and the analytical failure load (10.524 kN) calculated from Eq. (12). The error between the two values is only 1.18%, which reflects the plausibility of the material model and the ice material properties.

The comparison between model predictions and empirical data/models indicates that the MAT 124 model shows good performance in predicting the uniaxial compressive strength and flexural strength of the ice. Hence, this model is further used in simulations of ship-ice interactions.

3.3 Simulation and verification of ice loads during ship-ice interaction

The generation of ice loads should be closely related to the relevant ice failure mode, especially during the loading stage [10]. In this section, the numerical model forming the basis for simulating the ship-ice interaction is outlined. The focus is on the primary impact loads, and thus, secondary interactions of broken ice pieces with the hull are disregarded.

The bow of the icebreaker Xuelong 2 (Fig. 8 (a)) is modeled by means of rigid shell finite elements (as shown in Fig. 8 (b)), the level ice is discretized with solid elements, and MAT 124 is deployed with the parameters reported in Table 2 (Section 3.1). For simplicity, a homogenous ice field is assumed.

The model for simulating the ship-ice interaction is shown in Fig. 9. In this model, the effects of seawater on the behavior of the ship and ice are considered by applying the Arbitrary Lagrangian Eulerian (ALE) method, and the relevant details can be found in Appendix B.

(a) The Xuelong 2 icebreaker
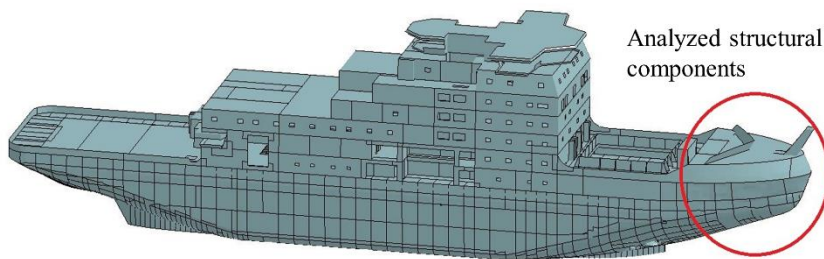
(b) Analyzed structural components

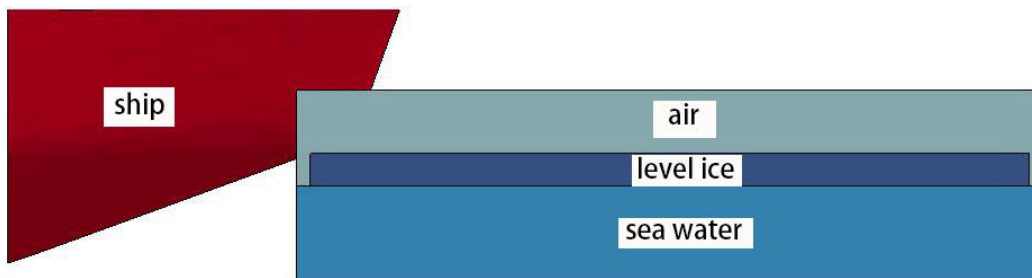Fig. 8 Model of the Xuelong 2 icebreaker to be analyzed

Fig. 9 The model for simulation of ship-ice interaction

According to the operational characteristics of Xuelong 2, a speed of 3 knots and an ice thickness of 1.0 and 1.5 meters are applied [25]. The width of the level ice model is 80 m, which is almost 4 times the hull width, and the length of the model is set to 80 m. To obtain convergent results while retaining a reasonable CPU time, the element mesh of the level ice is set to $400 \times 400 \times 400$ mm (the element convergence analysis was carried out in section 4.1). The degrees of freedom in the x- and y-directions at the ice boundary are fixed. In this paper, a case with 2726-m long level ice is divided into

60 cases, which includes ships, parts of the level ice and the water, as shown in Fig. 9.

Then, long sequences of time-domain simulations representing the ship-ice interaction process are obtained by reconstructing long-duration signals from a series of short-duration simulations. The preload is established by means of a separate step of the analysis, as described in Section 2.1.

Since full-scale test data of Xuelong 2 are not available, the simulated ice loads cannot be directly validated. Instead, the Xuelong 2 designed ice pressure, in accordance with the China Classification Society (CCS) rules, is used to assess the magnitude of the simulated ice loads. The details of the design ice pressure calculations can be found in Appendix C.
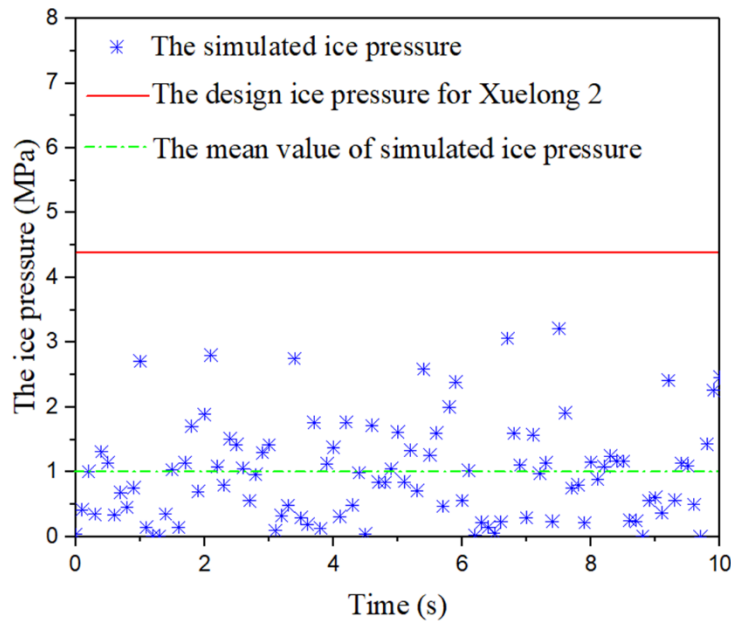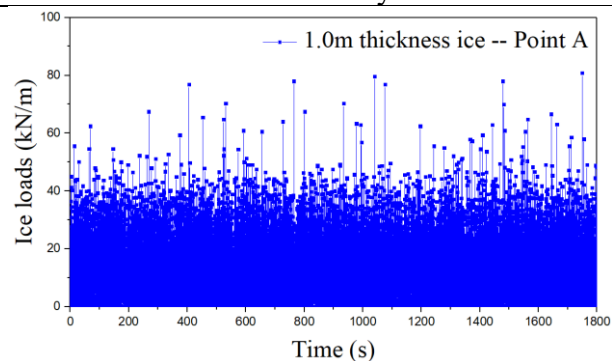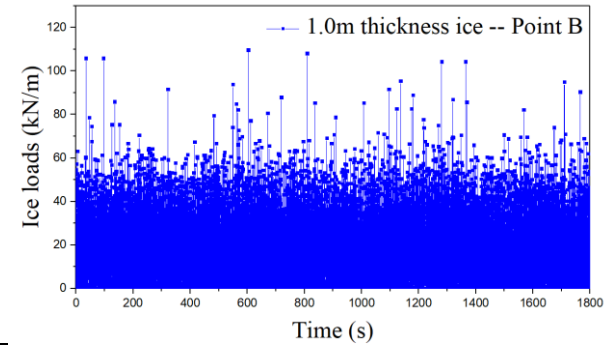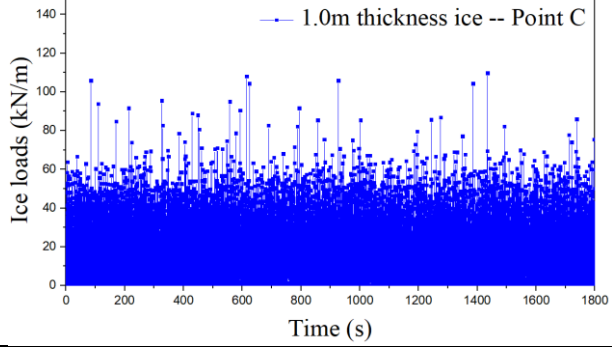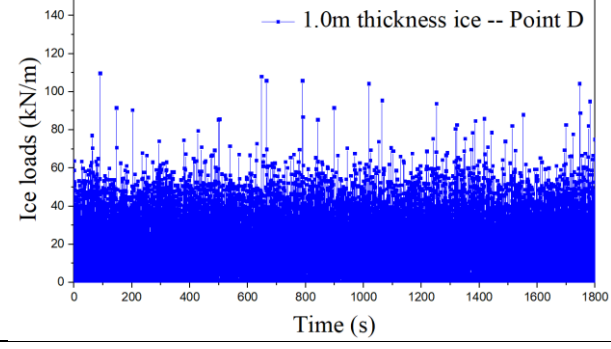

Fig. 10 Magnitude of simulated pressure versus designed ice pressure

Fig. 10 presents the designed ice pressure and the simulated ice pressure. The designed ice pressure of the CCS is approximately 4.4 MPa, and the simulated ice pressure is approximately 0~3 MPa with a mean value of 1 MPa. Clearly, the simulated ice pressure is lower than the designed ice pressure. Classification societies usually provide conservative results under specified conditions during the design stage, so the difference between the designed and simulated values is reasonable.

3.4 Extreme value statistics of ice loads

Table 3 presents the number of line load peaks, the mean values, and the standard deviations of the peaks at different locations under the two different short-term conditions. Table 3 shows that the number of line load peaks for the 1.0-m ice thickness is higher than that for the 1.5-m ice thickness, while the mean value and the standard deviations for the 1.0-m ice are less than those for the 1.5-m thick ice. This result is consistent with the FDA ICE [4]. Furthermore, it is worth noting that the local ice loads are location dependent in this application example. For instance, the number of line load peaks at points A and F is higher than that at other points, while the mean values and standard deviations at points A and F are less than those at the other points.

Table 3 The spatial dependency of local ice loads

| 1.0-m ice thickness				
Location	Time history	N	Mean	Std
Point A		3992	15.643	30.428
Point B		3786	22.156	32.185
Point C		3046	25.264	33.416
Point D		3067	26.143	33.146

Location	Time history	N	Mean	Std
Point E		3803	21.983	32.198
Point F		3986	15.349	30.951
1.5-m ice thickness				
Location	Time history	N	Mean	Std
Point A		3114	23.042	45.440
Point B		2953	32.630	46.773

Point C		2376	37.861	48.766
Point D		2407	38.165	49.165
Point E		3004	32.156	47.016
Point F		3168	22.861	44.591

where N denotes line load peaks for two short-term cases, Mean denotes mean values (kN/m), Std denotes standard deviations (kN/m). The locations of the points are consistent with Fig. 3.

The obtained line load peaks were given as inputs to the ACER analysis [14], and the calculation results are shown in Fig. 11 and Fig. 12.
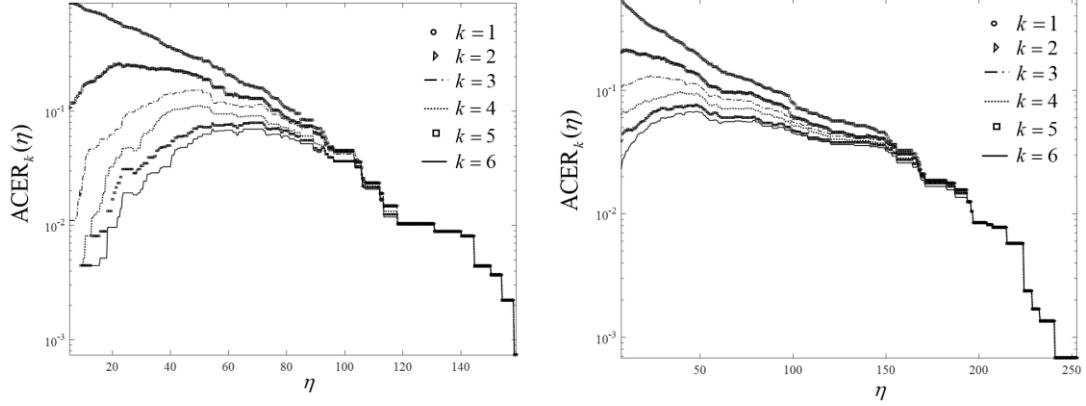
(a) 1 m   (b) 1.5 m

Fig. 11 ACER functions of different orders of k for the line load peaks
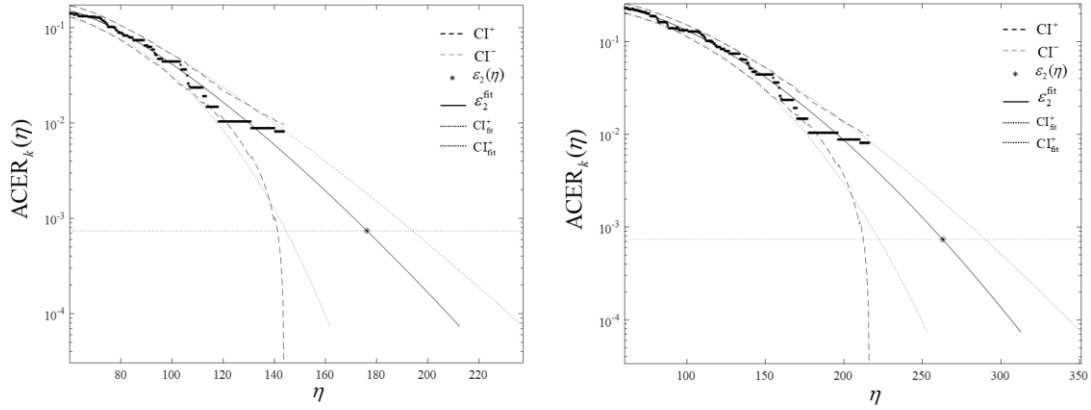
(a) 1 m   (b) 1.5 m

Parameters: a_2=0.0017, b_2=28.211,   Parameters: a_2=0.0008, b_2=42.316, c_2=1.694, q_2=0.255, η_0=40 c_2=1.701, q_2=0.256, η_0=60

Fig. 12 Extreme ice load at point C; prediction is based on the ACER function ($k=2$). The two points (marked as *) are the target extreme values.

The target exceedance probability for the two cases is specified as 0.1, i.e., $1-\text{Prob}(M_N \leq \eta)=0.1$. The corresponding 90% fractile values for two ice conditions can then be estimated by Eqs. (6) and (7). The results show that the 90% fractile value for the 1.0-m ice thickness condition is 176.486 kN/m, and the 1.5-m ice thickness condition has a higher value of 268.629 kN/m. It is accordingly found that more severe ice conditions imply a higher likelihood of experiencing larger ice loads, which is consistent with the expectations.

Subsequently, the ACER functions $\varepsilon_k(\eta)$ for different orders of k are obtained based on the ice loads for the two cases, as shown in Fig. 11 (a) and (b). The ACER functions of order $k = 2$ are selected, and the extreme values of the ice loads can then be estimated. Fig. 12 (a) and (b) illustrate the estimation of the extreme values at the target probability level by applying the ACER method. Moreover, the predicted ACER functions and the fitted 95% confidence intervals (CI) are also plotted in these two

figures.

3.5 Fatigue damage analysis

The purpose of this section is to illustrate the application of the developed simulation procedure to perform icebreaker fatigue assessment. Thus, for simplicity, only a single point (point C with the greatest line ice loads) is selected. The structural details of point C are shown in Fig. 13 (a) and (b).

(a) Location of the fatigue point
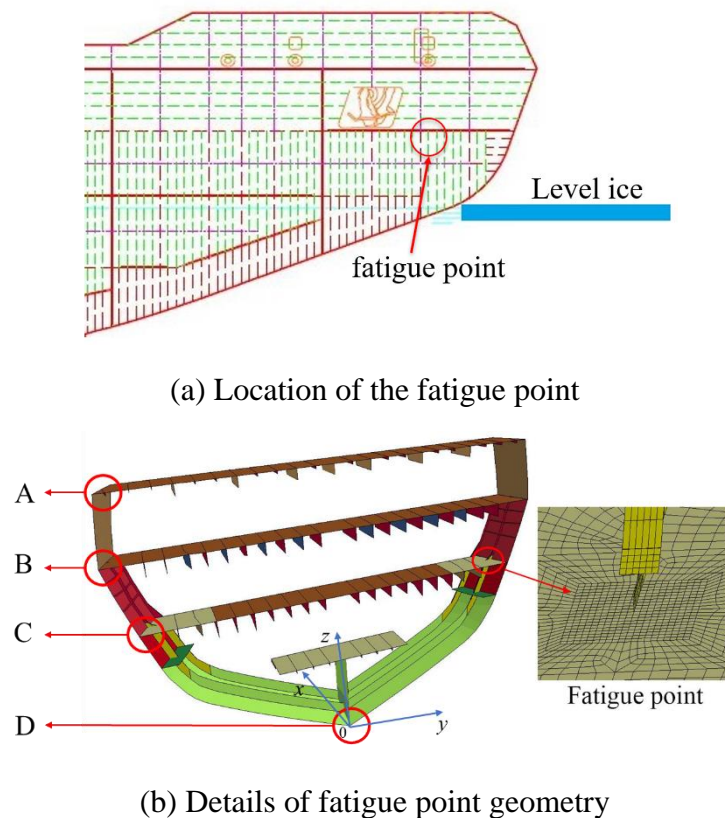

(b) Details of fatigue point geometry

Fig. 13 The fatigue point selected for fatigue damage analysis

The four connections (A~D) in Fig. 13 (b) are taken to represent simple supports (translations in the x-, y- and z-directions are zero, and all three corresponding rotations are nonzero). According to Section 2.2.3, the boundary condition c (with m_0=10.0) is chosen herein. Then, the transformation factor γ=0.225 (determined based on Eqs. (4) and (5)) is applied to calculate the corresponding stress based on Eq. (3).

Subsequently, the probability density function can be found by regression analysis based on the obtained stress ranges. The assumptions that are made about the type of probability density function that should be applied for the stress ranges have a significant influence on the estimated fatigue damage. The Weibull model, the Gumbel model and the lognormal model are all applied and compared with respect to fitting the probability density function of peak stresses based on the maximum likelihood estimation method. An overview of the mathematical expressions for the different density functions is given in Table 4 [26].

Table 4 Various probability density functions

Distribution	Probability density function
Gumbel	$f_s(S) = \dfrac{1}{\beta}\exp\{-\dfrac{(S-\alpha)}{\beta}\}\exp\{-\exp[-\dfrac{(S-\alpha)}{\beta}]\}$
Lognormal	$f_s(S) = \dfrac{1}{S\sqrt{(2\pi\sigma^2)}}\exp\{-\dfrac{(\ln S - \mu)^2}{2\sigma^2}\}$
Weibull	$f_s(S) = \dfrac{k}{\theta}(\dfrac{S}{\theta})^{k-1}\exp\{-(\dfrac{S}{\theta})^k\}$

The probability distributions are obtained by applying the peak stresses at the fatigue point for the two different ice thickness conditions. The probability densities corresponding to the analytical probability models and the histograms of the peak stresses are plotted in Fig. 14 (a) and (b). It can be seen that the results obtained by fitting with the Weibull distribution model are better than for the other models.

(a) The distribution for 1.0-m ice. (b) The distribution for 1.5-m ice.
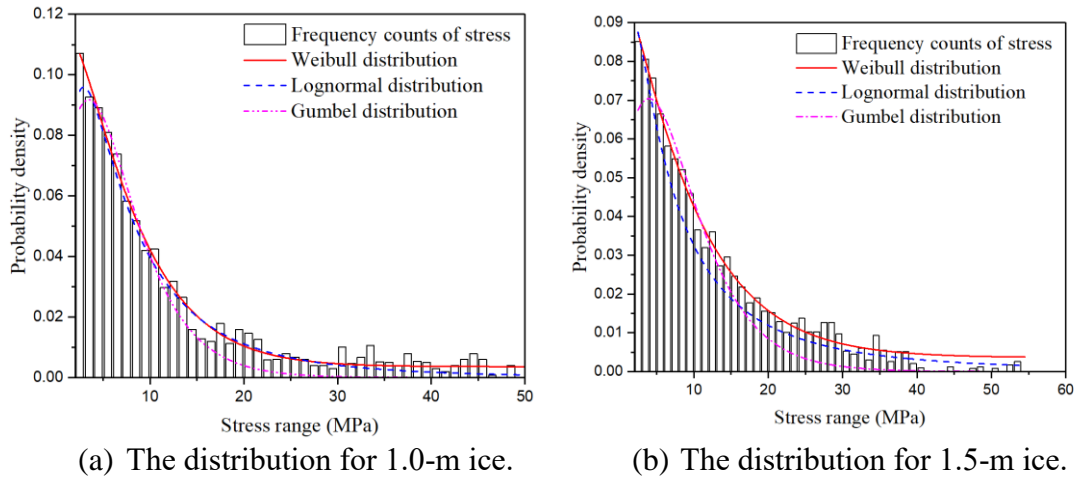Fig. 14 The distribution of peak stresses

In combination with Eq. (10), the fatigue damage during the stationary short-term conditions can be calculated based on a given probabilistic model.

Lloyd's Register applies S-N curves at room temperature for the fatigue damage analysis of typical welded joints at low temperatures [4]. Considering the influence of joint details on S-N curves, the F_2 curve [4] with $m=3$ and $C=1.23E+12$ is applied in this paper. The fatigue damage is computed based on the various probability models, which are presented in Table 5.

Furthermore, Lloyd's Register proposes a procedure for fatigue damage analysis [4]. The fatigue damage predicted by this procedure is also presented in Table 5. In this procedure, the distribution of ice load amplitudes is approximately described by a Weibull distribution. The scale parameter of the Weibull distribution for the ice load in the forward region of the hull is based on the following expression:

$$F = 93C_{form} \frac{(\Gamma(1+\frac{2}{\xi}) - \Gamma^2(1+\frac{1}{\xi}))^{0.52}}{\Gamma^{2.04}(1+\frac{1}{\xi})} \qquad (11)$$

where

F is the scale parameter of the Weibull distribution for the ice load (kN/m),

Γ is the gamma function,

ξ is the Weibull shape parameter, $\xi = 0.8h_{eq}^{-0.6}$, and

C_{form} is the hull form factor.

The number of ice impacts and ice loads for a sailed distance, D_n, in equivalent ice thickness h_{eq} [4] is expressed as:

$$N_t = \frac{D_n \cdot C_{region}}{10.4h_{eq}^{3/4} - 2h_{eq} + 1.18} \qquad (12)$$

where

h_{eq} is the equivalent ice thickness (m),

C_{region} is the hull region factor, which can be set to 1.0 in the forward part of the ship,

D_n is the sailed distance (m) in ice, and

N_t is the number of ice impacts for the sailed distance.

Table 5 Fatigue damage for the stationary short-term conditions of 1800 s duration

Calculation method	Fatigue damage ($\times 10^{-7}$)	
	1.0-m thickness	1.5-m thickness
Gumbel distribution	59.152	183.761
Weibull distribution	89.759	373.53
Lognormal distribution	61.465	297.723
Histograms	72.027	216.737
FDA ICE	92.762	436

Table 5 shows that the fatigue damage results calculated by the FDA ICE method are higher than those for the other models and histograms. This is because the scale parameter of the Weibull distribution for the ice load of the FDA ICE method is based on an empirical equation (Eq. (11)) rather than actual ice load conditions. Furthermore, the FDA ICE method is based on an ice-strengthened ship navigating in first-year ice conditions, while the hull of an icebreaker is stronger than a general ice-strengthened

ship. Therefore, it is reasonable that the fatigue damage of the icebreaker predicted by the FDA ICE method is higher than that obtained by the proposed procedure.

It is also seen that the fatigue damage predicted for the 1.0-m-thick ice is less than that for the 1.5-m-thick ice. This result is related to the differences in terms of the number of impacts and the amplitudes of the ice loads. In general, the frequency of line load peaks decreases with increasing ice thickness, while the magnitudes of the peaks increase with increasing ice thickness [4]. According to the procedure given by Lloyd's Register, the number of impacts and the amplitudes of the ice loads are related to the ice thickness (Eq. (11) and Eq. (12)) [4].
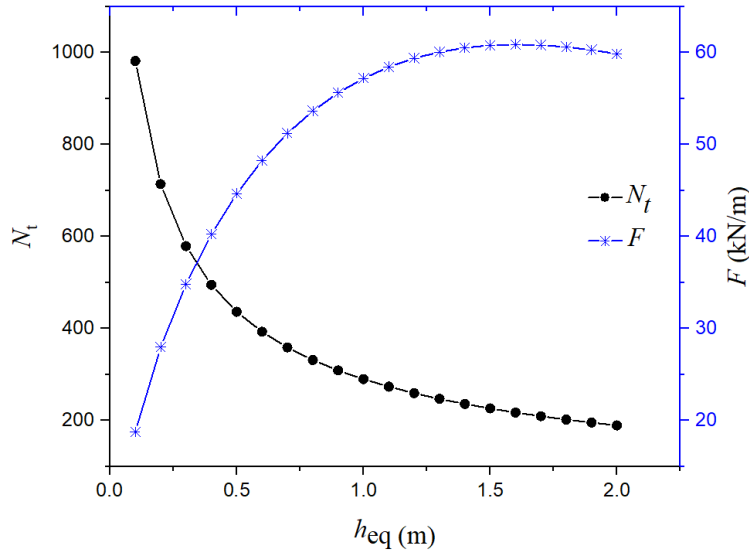

Fig. 15 The number of ice impacts and line load magnitude for a sailed distance as a function of equivalent ice thickness (the sailed distance is 2777.76 m, which is obtained by multiplying 1800 s duration by 3 kn speed) [4]

The relationships among the number of ice impacts, ice loads and equivalent ice thickness also agree with the results obtained in the present study, as shown in Fig. 15. Fatigue damage is clearly influenced by both the number of ice impacts and the magnitude of the ice loads.

According to Eq. (12), the parameter N_t is a "linear" proportionality factor with respect to the fatigue damage. Furthermore, there is a linear relationship between ice loads and fatigue stresses. Accordingly, the parameter F in Eq. (11), which can be regarded as a scaling factor for the stress, enters the fatigue damage calculation in terms of a power function (i.e. $(F \times \gamma)^m, m > 1$). This implies that the effect of an increase of the scale factor F is higher than for a similar percentwise increase of the parameter N_t. Therefore, although the number of ice impacts for the 1.0-m-thick ice is larger than that for the 1.5-m-thick ice, the fatigue damage for the former case is smaller than that for the latter case.

4 Discussion

The purpose of this paper has been to provide researchers and engineers with a procedure for a probabilistic fatigue damage assessment of ships moving through a level ice field. A novel six-step procedure for fatigue damage assessment using numerical simulations is proposed. To illustrate the procedure, a hypothetical scenario with the Xuelong 2 icebreaker and an 'example' ice model has been provided. The proposed procedure is not limited to the ice model or to the ship-ice interaction modeling technique and can be used along with other modeling approaches (see, e.g., [27]) provided the convergence of the calculation results can be demonstrated.

While statistical methods for fatigue assessment have received a great deal of attention, phenomenological ice modelling techniques have not. The latter also includes numerical techniques for simulating the ice fragmentation process (e.g., spalling, comminution) and benchmarking the different ice modeling techniques. Researchers can benefit from more precise ice model formulations, accounting for viscous effects, pressure-dependent behaviors, inhomogeneities and the post fracture behavior of ice within the ship-ice-water-air system.

Furthermore, it is worth noting that the thickness and the properties of the level ice are taken as equivalent constants in this paper. Actually, the thickness and properties of level ice are random in the Arctic region [2, 10]. For example, Chai et al. found that the ice thickness is nonstationary based on short-term full-scale measurements in the area around the Svalbard Islands [2]. The reference period for the ice load needs to be extended if the thickness and properties of the level ice are represented as random values. Numerical simulations of ice loads and fatigue damage with random ice thickness and random ice properties deserve more detailed studies as part of future research.

Apart from the ice modeling assumptions and treatment of the ice-structure water interaction problem, many other factors can affect the results of fatigue damage. The discussion below pertains specifically to the following aspects: the analysis of numerical convergence (discretization errors), the reference period, the effect of boundary conditions, and the S-N curves. The results of fatigue damage in the Discussion are predicted based on the Weibull distribution from Section 3.5.

4.1 Analysis of numerical convergence

A fatigue damage analysis is carried out based on a numerical simulation of ship-ice interaction, so the estimated fatigue damage can be sensitive to some of the numerical parameters, including the element size applied for representation of the level ice and the reference period for the ice loads. As a first step in the present study, an element convergence analysis is carried out.

Due to the stochastic nature of the ice-induced loads, it can be difficult to analyze the element convergence based on the simulated time series directly. As a more stable measure, the accumulated damage at the fatigue point is chosen to study the element convergence properties. Five groups of element sizes are chosen to build the level ice in the model, and the corresponding fatigue damage as well as the CPU time with 8 cores are calculated and recorded, as shown in Fig. 16. Fig. 20 shows that the fatigue

damage increases and the CPU time decreases with increasing element size. To obtain convergent results with an acceptable CPU time, the element size representing the level ice is set to $400 \times 400 \times 400$ mm.
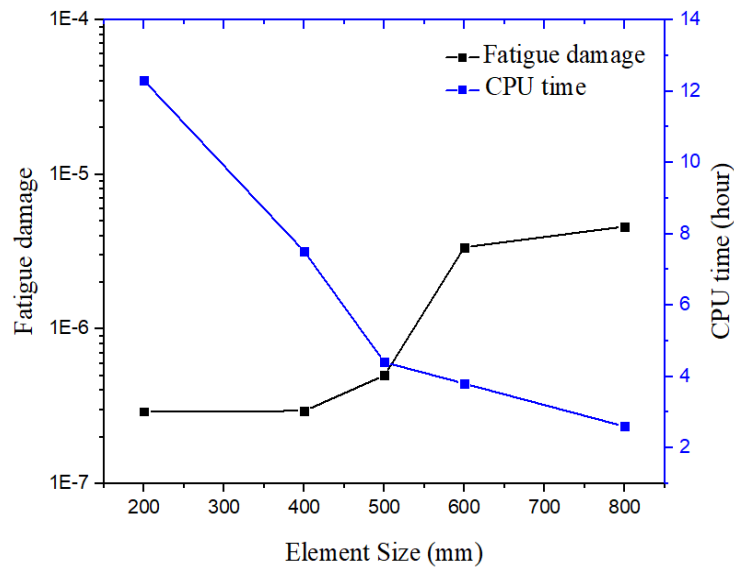

Fig. 16 Results of the element convergence analysis

(System characteristics: 8 processors, 2.30 GHz)

4.2 Reference period

Furthermore, the reference period for the ice load can affect the parameters of the probability distribution model [28]. The effect of the reference period on the fatigue damage is studied in this section. The parameters of the Weibull probability model are fitted based on different reference periods, and the results are shown in Fig. 17 (a) and (b). It can be seen that the value of θ decreases when the reference period increases from 300~1200 and tends to stabilize after 1200 s. The parameter k also gradually converges after 1200 s for the two different ice thickness conditions.
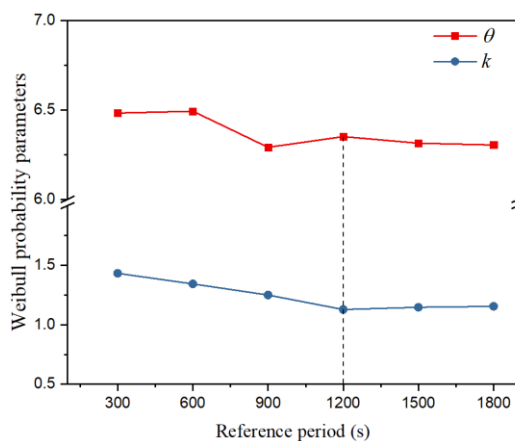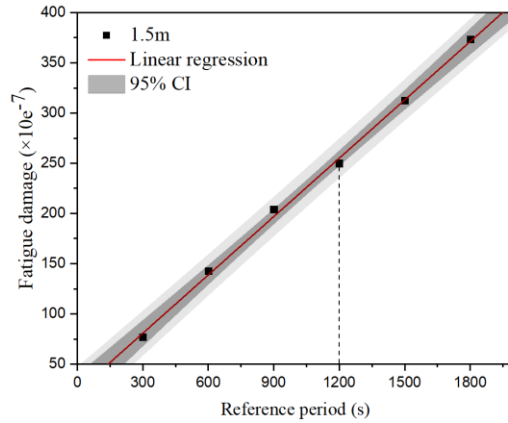

(a) Parameters of the Weibull probability model for the 1.0-m thickness condition
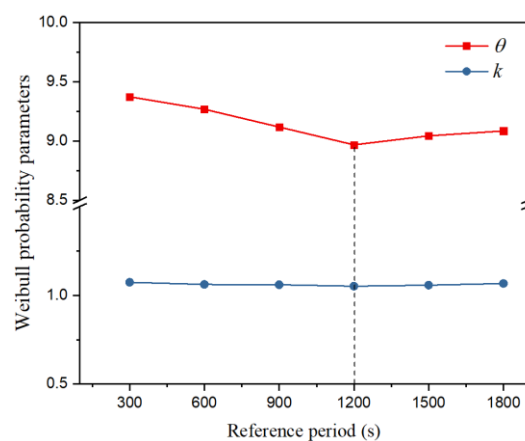
(b) Parameters of the Weibull probability model for the 1.5-m thickness condition

25
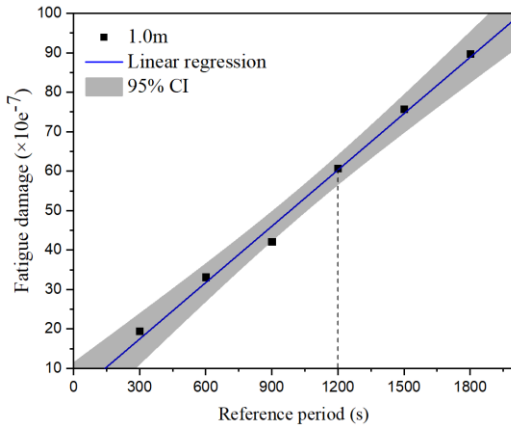
(c) Fatigue damage for the 1.0-m thickness condition

(d) Fatigue damage for the 1.5-m thickness condition

Fig. 17 Parameters of the Weibull distribution, (a) and (b), and fatigue damage for different reference periods, (c) and (d).

Subsequently, the fatigue damage for different reference periods is calculated, as shown in Fig. 17 (c) and (d). The fatigue damage and the reference period exhibit a linear relationship based on the present results. The fitted linear relationship in the figure implies an increase in the damage as a function of the reference period, which essentially becomes perfectly linear after 1200 s. Therefore, in the present study, a 1200-s reference period is selected for the ice load for the purpose of fatigue damage analysis.

4.3 The effect of boundary conditions on fatigue damage

Eqs. (3) and (8) show that the fatigue stress at the fatigue point is proportional to the transformation factor γ, which implies that changing this factor has a strong influence on the resulting fatigue damage. According to Eqs. (4) and (5), the transformation factor γ is related to the boundary coefficient m_0. Therefore, the selection of boundary conditions is important with respect to the resulting fatigue damage. In this section, the effect of the boundary condition on the computed fatigue damage is addressed.

Table 6 The boundary conditions and transformation factor considered in the present study.

(The notation x=y=z=0 means fixed translations and Rx=Ry=Rz=0 means fixed rotations)

	Boundary Condition		
	a	*b*	*c*
A	$x = y = z = 0,$ $Rx = Ry = Rz = 0$	$x = y = z = 0,$ $Rx \neq Ry \neq Rz \neq 0$	$x = y = z = 0,$ $Rx \neq Ry \neq Rz \neq 0$

B	free	free	$x = y = z = 0,$ $Rx \neq Ry \neq Rz \neq 0$
C	free	free	$x = y = z = 0,$ $Rx \neq Ry \neq Rz \neq 0$
D	$x = y = z = 0,$ $Rx = Ry = Rz = 0$	$x = y = z = 0,$ $Rx = Ry = Rz = 0$	$x = y = z = 0,$ $Rx \neq Ry \neq Rz \neq 0$
m_0	8	5.3	10
γ	0.281	0.425	0.225

Table 6 lists three different boundary conditions that are presently considered. The values of the computed fatigue damage corresponding to the different boundary conditions are shown in Fig. 18. It can be seen in this figure that the fatigue damage increases with the value of γ, which is clearly due to the increase in the stress level at the fatigue point. In short, the resulting fatigue damage is significantly affected by boundary conditions. Accordingly, these should be chosen very carefully when the fatigue stress is predicted based on beam theory.
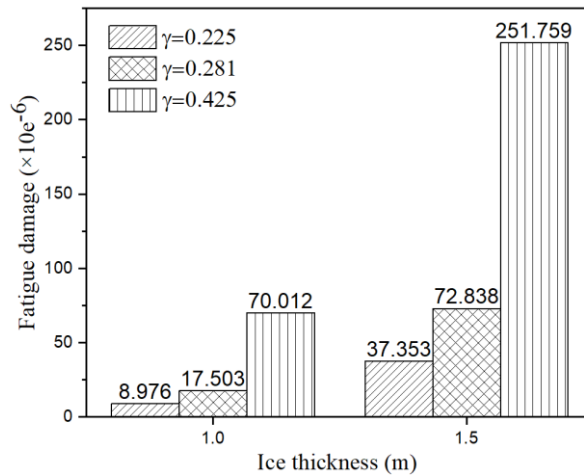

Fig. 18 The effect of the transformation factor γ on the estimated fatigue damage

4.4 Application of the low-temperature S-N curve for fatigue damage analysis

It is well known that temperature is one of the most influential environmental parameters that affect the behavior of materials [29]. Relevant research has shown that the S-N curves can also be affected by temperature [30]. Apparently, the ambient temperature in the Arctic region is lower than room temperature (20 ℃) [31]. Therefore, the effect of applying low-temperature S-N curves deserves to be studied. This section aims to investigate the effect of applying low-temperature S-N curves on the results computed by application of the proposed procedure.

First, the ambient temperature for the S-N curves should be determined based on the surface air temperature during the passage. One of the sailing routes of Xuelong 2 is the Arctic Northeast Passage, which follows the Russian and Norwegian coasts (Fig.

19 (a)). The surface air temperature during the passage is approximately 0 °C (daytime, from July to September 2018), as shown in Fig. 19 (b).
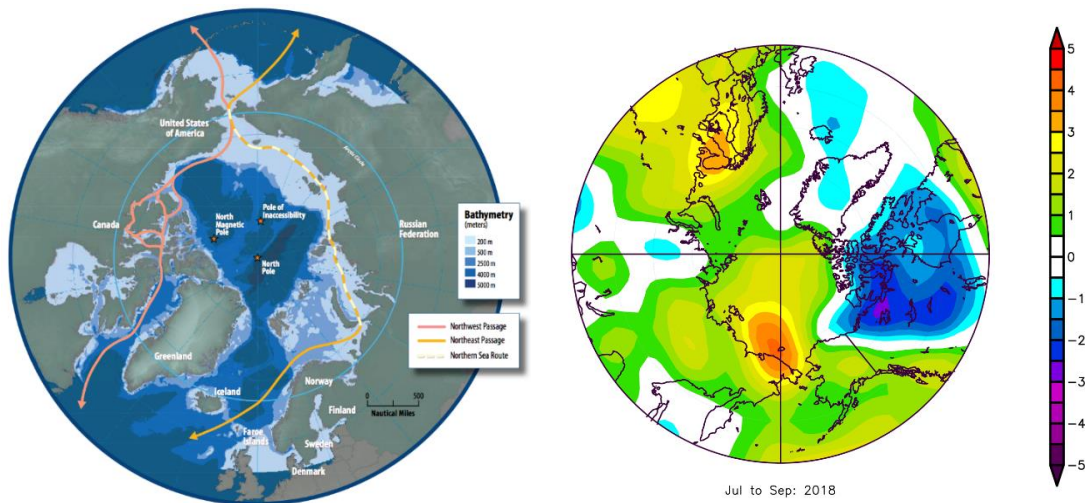

(a) The passage of Xuelong 2 in the Arctic region [31]

(b) The surface air temperature in the Arctic region (daytime, July to September 2018)

[Data for this figure are available from NOAA/ESRL, Boulder, CO, at https://www.esrl.noaa.gov/psd/]

Fig. 19 The route for the passage and the temperature for Xuelong 2 in the Arctic region

Fatigue tests are carried out at low temperatures to obtain relevant S-N curves. The material used for the specimens is DH36 (certified by ABS). The specimens are designed by referring to the "ASTM E466-15 Standard Practice for Conducting Constant Amplitude Axial Fatigue Tests of Metallic Materials" [32]. The characteristics of the size and geometry of the longitudinal fillet welded joint specimen are shown in Fig. 21(a). The fatigue tests are performed at 0 °C. The temperature is controlled using a low-temperature environmental chamber (Fig. 20 (b)).
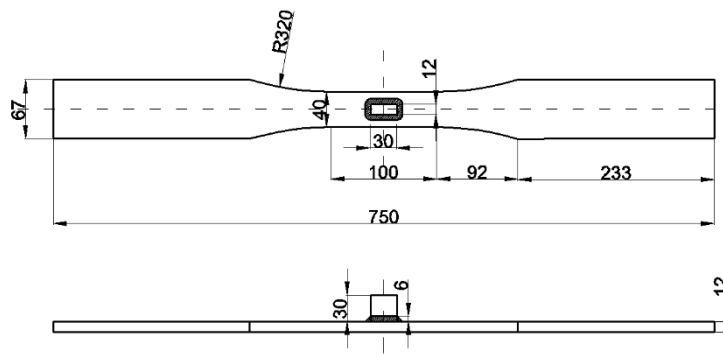
(a) Longitudinal fillet welded joints (unit: mm)
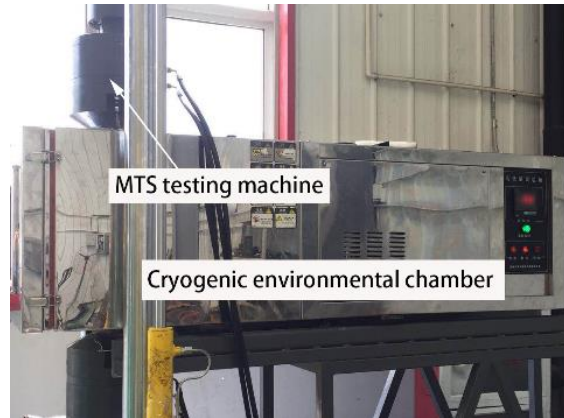
(b) Testing setup

Fig. 20 Detailed drawing of the fatigue test at low temperatures

For the S-N curves at 0 ℃, the raw data and double logarithmic S-N curves corresponding to two different confidence levels are shown in Table 7. The data processing is not given in detail herein, but a further description can be found in reference [33].

Table 7 Double logarithmic S-N curve with confidence level

0℃	
50% confidence level	$\lg N = 12.901 - 3\lg S$
95% confidence level	$\lg N = 12.772 - 3\lg S$

When comparing this S-N curve with two other S-N curves [4] [34] applied at room temperature (Fig. 21), it can be seen that the S-N curve at 0 ℃ (95% confidence level) is located above the two other curves, which means that the low temperature increases the fatigue strength of the present material. A fatigue damage analysis is subsequently carried out based on the three S-N curves in Fig. 21. The results are presented in Table 8, and it can be seen that the fatigue damage estimated based on the S-N curve for low temperature is approximately 20~25% of the fatigue damage

29

estimated based on the S-N curves for room temperature. This applies to both ice thickness conditions. The S-N curves at room temperature are applied to the fatigue damage evaluation of polar structures by applying the relevant design procedures, such as Lloyd's Register Ship Right Design and Construction [4]. These S-N curves lead to more conservative results during the design phase of such structures for safety reasons. Relevant S-N curves for low temperatures can accordingly provide a more accurate prediction of fatigue damage during the evaluation phase for polar structures.
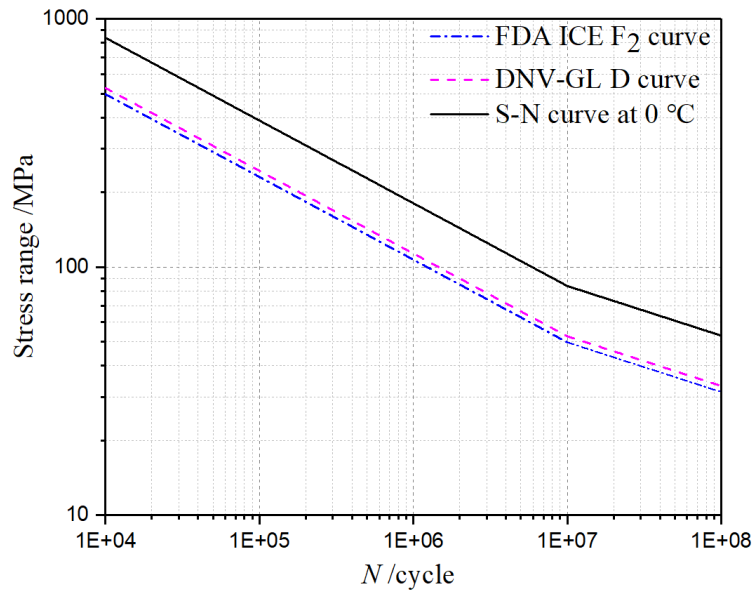

Fig. 21 S-N curves

Table 8 Fatigue damage obtained by application of different S-N curves
(reference period: 1800 s; point C)

Ice thickness (m)	Fatigue damage for different S-N curves (×10e-6)		
	FDA ICE F_2 curve	DNV-GL D curve	S-N curve at 0°C
1.0	8.976	6.198	2.48
1.5	37.353	34.168	5.741

5 Conclusions

Icebreakers represent an important class of vessels in relation to activities in polar regions. Fatigue damage assessments of these vessels during operations in various ice conditions are important to maintain an adequate safety level. This study provides researchers and engineers with a simulation-based procedure for a probabilistic fatigue damage assessment of ships moving through a level ice field. To illustrate the proposed procedure, a numerical example in relation to Xuelong 2 has been provided by focusing only on the primary ice impact loads (ice crushing and flexural failure). The results obtained as part of the present study lead to the following conclusions:

(1) A 1200-s reference period can provide convergent Weibull parameters and fatigue damage for ship navigation in level ice fields. For other ice fields, the reference period can be different.

(2) Applied boundary conditions in relation to the calculation of stresses at the fatigue point have a strong influence on the computed fatigue damage. For example, the fatigue damage with boundary condition b is almost 6.7 times that of boundary condition c for a 1.5-m ice thickness condition. The boundary conditions should accordingly be carefully selected when fatigue stresses are predicted by beam theory.

(3) It is found that the S-N curve at room temperature leads to more conservative results. The fatigue damage calculated based on the S-N curves corresponding to 0°C is only approximately 15% of the fatigue damage calculated based on the FDA ICE F_2 curve and the DNV-GL D curve. This inherent conservatism is likely due to consideration of safety in the case that relevant fatigue data are lacking. If adequate information is available, the selection of the S-N curves can instead be based on more realistic conditions with respect to fatigue damage evaluation at low temperatures.

Future work should focus on evaluating the fatigue damage for different ice conditions (e.g., broken ice, deformed ice, brash ice, etc.), ice thermal states, and ice ages under different ice model assumptions. Furthermore, re-emphasize the need of a modeling approach for long-term fatigue analysis also should be studied. The question of how to incorporate the most advanced state-of-the art ice mechanics into the proposed fatigue assessment procedure and the corresponding implications should also be addressed.

Appendix A: The ice material model and its verification
Appendix A.1 The ice material model
Material Type 124 *MAT_PLASTICITY_COMPRESSION_TENSION is an isotropic elastic-plastic material where unique yield stress versus plastic strain curves can be defined for compression and tension [17]. Additionally, failure can occur based on a plastic strain or a minimum time step size. Rate effects in relation to the yield stress are modeled either by using the Cowper-Symonds strain rate model or by using two load curves that scale the yield stress values in compression and tension, respectively.

However, only the effect of rate on compressive stress is considered by defining a strain rate vs compressive yield stress scale factor (CYSF) curve in this study. Mean stress is an invariant that can be expressed as $(\sigma x + \sigma y + \sigma z)/3$.

Furthermore, the isotropic elastic-plastic material allows unique yield stress versus plastic strain curves to be defined for compression and tension. The curves of yield stress (σ_y) vs effective plastic strain (ε_p) in both tension and compression are established based on the following equation:

$$\sigma_y = \sigma_y^0 + E_p \varepsilon_p \tag{A1}$$

where

σ_y^0 is the initial yield strength (MPa) and

E_p is the plastic hardening modulus (GPa).

The effective stress versus effective plastic strain in compression and tension is defined in Fig. A1.
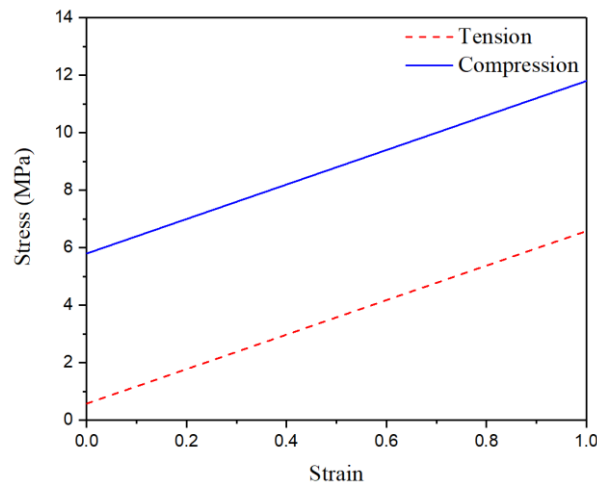
Fig. A1 yield stress versus plastic strain curves in compression and tension

To formulate the strain rate vs compressive yield stress scale factor (CYSF) curve, initially, the compressive strengths at different strain rates are determined from the following equation given by Sanchez [35].

$$\sigma_c^0 = 10976 \dot{\varepsilon}^{0.093783} \tag{A2}$$

The initial yield strength in tension σ_t^0 is assumed to be 10 times less than σ_c^0.

The compressive strengths are further normalized with the compressive strength (5.8 MPa) at 10-3 s-1. The strain rates and the corresponding compressive yield stress scale factors (CYSFs) are shown in Fig. A2.

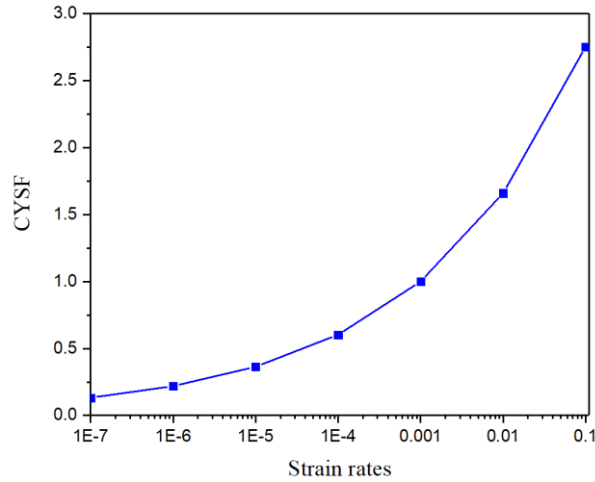Fig. A2 Strain rate vs compressive yield stress scale factor (CYSF) curve

Appendix A.2 Compressive failure of ice

It is well known that ice compressive strength in a confined ice sheet is much higher in magnitude than for a full width loading of a thinner ice sheet [36]. Therefore, the confinement of ice should be determined before performing simulation of the behavior in compression. Based on the flat jack test data from Iyer and Masterson [37], the confinement coefficient for different geometries is obtained. This can be illustrated as shown in Fig. A3(a). In addition, $t/\sqrt{A}$ is less than 0.3, which implies that a uniaxial state model can be applied (the value of $t/\sqrt{A}$ can be estimated based on the simulation in Section 3.3). Accordingly, a uniaxial compression model of the ice is applied in the numerical simulations.

There are three different "subsystem models" that can affect the compressive simulation study: the ice cylinder itself, the rigid upper support and the lower support of the cylinder. According to the research by Schwarz [35], the suggested dimensions of a uniform standard uniaxial compressive specimen are 70 mm in diameter and 175 mm in length. The dimensions of the ice cylinder suggested by Schwarz are adopted for the simulation of compressive strength (Fig. A3(b)). The MAT_ PLASTICITY_COMPRESSION_TENSION material model, which is the same as the model in Section 3.1, is chosen for the ice mass within the cylinder.

Furthermore, CONTACT_ERODING_SURFACE_TO_SURFACE is applied for the contact between the ice cylinder and the rigid supports to automatically eliminate any element that reaches the failure criteria during a simulation. The static friction coefficient is assumed to be 0.1 between the ice and the rigid supports. The lower support is fixed with six degrees of freedom, and the upper support is fixed with five degrees of freedom and moves downwards with constant velocity.
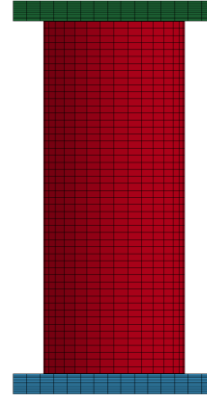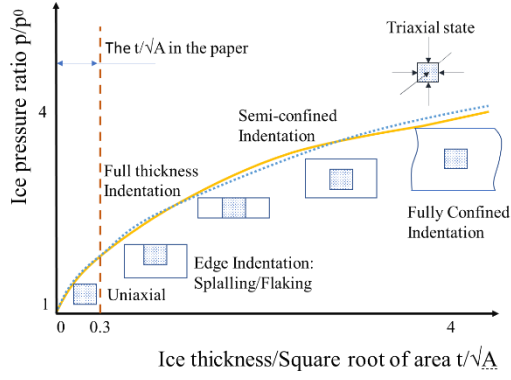
(a) The loading regimes for compression (where t is the ice thickness, A is the loaded area, P is the ice pressure, and P_0 is the ice pressure under uniaxial conditions) [36]

(b) The FEM model

Fig. A3 The model for simulating compressive loading

Timco and Frederking developed a model to calculate the strength of sea ice sheets. They derived equations for the uniaxial compressive strength of first-year sea ice for several different grain structures. The uniaxial strength of first-year sea ice is [22, 23]

$$\sigma_c = 37(\dot{\varepsilon})^{0.22}[1 - \sqrt{\frac{v_{\mathrm{T}}}{270}}] \qquad (A3)$$

where

σ_c is the uniaxial compressive strength (MPa),

v_{T} is the porosity of the ice in parts per thousand, and

$\dot{\varepsilon}$ is the strain rate.

Appendix A.3 Flexural failure of ice

The finite element model for flexural simulation consists of three parts: the solid sea ice beam model and the rigid upper and lower supports modeled by means of eight-node brick elements, as shown in Fig. A5(a). The dimensions (L×B×H) of the ice beam are set as 4320×365×392 mm. The bending supports at the upper side are spaced 2 m from the beam center, while the supports at the lower side of the beam are spaced 0.5 m from the center. In addition, there is no shear force between the bottom rigid supports (Fig. A5(b)). The material model and ice material properties are consistent with those in Section 1.1.

Furthermore, the CONTACT_AUTO_SURFACE_TO_SURFACE keyword is adopted, and the static friction coefficient is assumed to be 0.1 between the ice and the rigid supports. The upper supports are fixed, whereas the load applying supports are free to move in the vertical direction (2.756 mm/s) only.
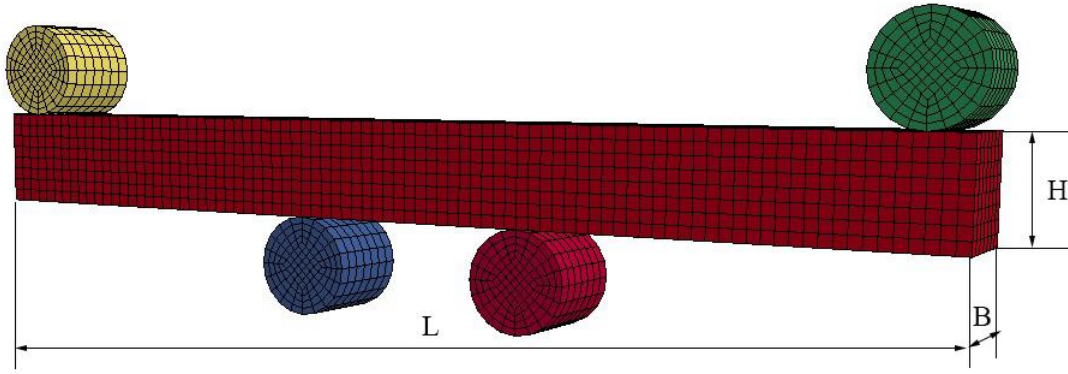
(a) The finite model for the ice beam
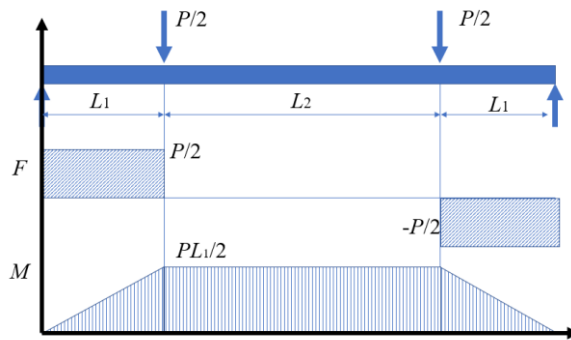
(b) Loading of the ice beam

Fig. A5 The bending model

Timco and O'Brien showed that the data for first-year sea ice can be described by [24]:

$$\sigma_f = 1.76 \exp(-5.88 \times \sqrt{v_b})$$ (A4)

where

σ_f is the flexural strength of the ice (MPa) and

v_b is the brine volume and is expressed as a brine volume fraction.

Appendix B: The effect of seawater

The effects of seawater on the behavior of the ship and ice can be considered by application of the Arbitrary Lagrangian Eulerian (ALE) method. The equations of state (EOS) and material model for sea water and air are implemented in LS DYNA. An EOS such as the Gruneisen model is suggested to simulate fluid domains in the current FE solver. The Gruneisen equation of state with cubic shock velocity-particle velocity defines the pressure for a compressed material as [38],

$$p = \frac{\rho_0 C^2 \mu [1 + (1 - \frac{\gamma_0}{2})\mu - \frac{a}{2}\mu^2]}{[1 - (S_1 - 1)\mu - S_2 \frac{\mu^2}{\mu+1} - S_3 \frac{\mu^3}{(\mu+1)^2}]} + (\gamma_0 + \alpha\mu)E \qquad (B1)$$

where E is the internal energy per initial volume and C is the intercept of the $\mu_s - \mu_p$ curve (speed of sound in water). S_1, S_2 and S_3 are the coefficients of the slope of the $\mu_s - \mu_p$ curve, γ_0 is the Gruneisen gamma parameter, and α is the first-order volume correction to γ_0. The seawater characteristics based on the relevant parameters are given in Table B1.

Table B1 The parameters for seawater [39]

Density, ρ_{water} kg/m^3	speed of sound in water, C m/s	S_1	S_2	S_3	γ_0
1030	1490	1.79	0	0	1.65

The elements of both the air and the water domains are assigned to the so-called null hydrodynamic material type that allows a new equation of state to be specified. The null hydrodynamic material type is material type (MAT_NULL) in LS DYNA [17]. MAT_NULL is used to model the fluid material. In the case of solids and thick shells, this material allows equations of state (EOS) to be considered without computing deviatoric stresses. Optionally, a viscosity can be defined. Additionally, erosion in tension and compression is possible.

An EOS with a polynomial form is used to define the initial thermodynamic state of the material and pressure, which is given by [38]:

$$p = C_0 + C_1\varsigma + C_2\varsigma^2 + C_3\varsigma^3 + (C_4 + C_5\varsigma + C_6\varsigma^2)E_0 \qquad (B2)$$

where $C_0 \sim C_6$ are user-defined constants, E_0 is the initial energy per initial volume, and ς is the volumetric parameter. The characteristic parameters corresponding to air are given in Table B2.

Table B2 The characteristic parameters for air [39]

Density, ρ_{air} kg/m^3	C_0	C_1	C_2	C_3	C_4	C_5	C_6	E_0 MPa
1.29	0	0	0	0	0.4	0.4	0	0.25

Appendix C: The design ice pressure

Xuelong 2 is a Chinese icebreaking research vessel that entered service in 2019. The ice class of Xuelong 2 is Polar Class 3 (PC3), and she is able to break ice up to 1.5

meters (4.9 ft) thick while traveling either ahead or astern. CCS specifies the design ice pressure [16], which can be used to compare with the simulated ice loads in this study.
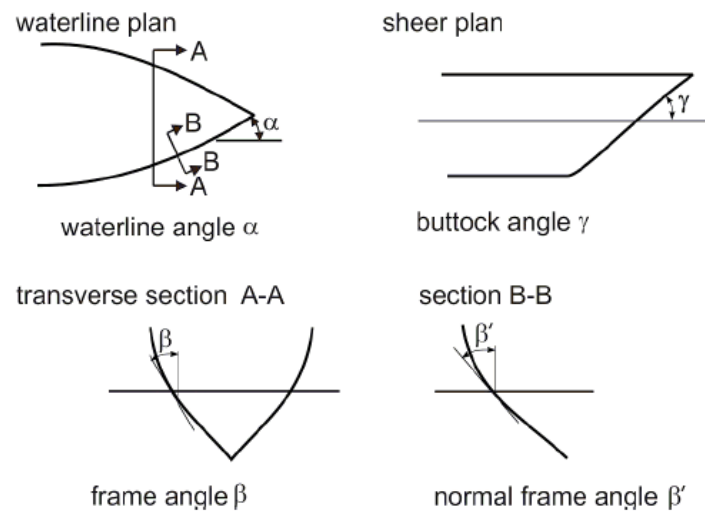

Fig. C1 The definition of hull angles [16]

Here,

$\beta^{'}$ is the normal frame angle in degrees,

α is the waterline angle in degrees, and

γ is the buttock angle at the high waterline in the ice area.

The hull angles also follow the relationships $\tan(\beta) = \tan(\alpha)/\tan(\gamma)$ and $\tan(\beta^{'}) = \tan(\beta) \cdot \cos(\alpha)$.

In the bow area, the design ice pressure is a function of hull angles. The effect of hull angles can be considered by the shape coefficient fa_i. The definition of hull angles is shown in Fig. C1.

The shape coefficient fa_i is written as

$$fa_i = \min(fa_{i,1}, fa_{i,2}, fa_{i,3}) \tag{C1}$$

where

$$fa_{i,1} = \frac{[0.097 - 0.68(\frac{x}{L} - 0.15)^2]\alpha}{(\beta^{'})^{0.5}}$$

$$fa_{i,2} = \frac{1.2CF_F}{\sin(\beta^{'}) \cdot CF_C \cdot D^{0.64}}$$

$$fa_{i,3} = 0.6$$

37

The force in MN is given by Eq. C (2),

$$F = fa_i \cdot CF_C \cdot D^{0.64} \tag{C2}$$

The parameter AR is

$$AR = 7.46\sin(\beta') \geq 1.3 \tag{C3}$$

The line loads Q in MN/m,

$$Q = F^{0.22} \cdot \frac{CF_D}{AR^{0.35}} \tag{C4}$$

The pressure P in MPa can also be taken as the maximum pressure

$$P = F^{0.22} \cdot CF_D^2 \cdot AR^{0.3} \tag{C5}$$

where

L is the length of the hull,

x is the distance between the first perpendicular FP and the calculated station,

D is the displacement of the hull,

CF_C is the crushing failure class factor, which can be taken as 6.16 for a PC 3 class icebreaker,

CF_F is the bending failure class factor, which can be taken as 21.17 for a PC 3 class icebreaker, and

CF_D is the load plate size ship class factor, which can be taken as 1.53 for a PC 3 class icebreaker.

The height of the load patch, b, is defined as

$$b = Q / P \tag{C7}$$

The required minimum shell plate thickness, t, is defined as,

$$t = t_{net} + t_s \tag{C8}$$

The thickness required to resist the ice loads on the structure, t_{net} depends on the orientation of the framing. The thickness to account for corrosion and abrasion, t_s, is taken as 3.5 mm for PC3 class vessels. For transverse framed plating in the bow region, the required net thickness is given as

$$t_{net} = 500s[(AF \cdot PPF_P \cdot P_{avg})]^{0.5} / [1 + s / (2b)] \tag{C9}$$

where

s is the frame spacing in m,

38

AF is the hull area factor, where AF for the bow region of an ice class vessel such as PC3 is 1.0,

PPF_P is the peak pressure factor for the plating, which can be given as $PPF_P = (1.8 - s) \geq 1.2$ for transverse framed plating, and

R_{eH} is the yield stress in MPa, which is taken as 400 MPa in this study.

As the required net thickness, t_{net}, is already given as 35 mm, the design pressure P_{avg} can be deduced from Eq. (C9)

Appendix D: The comparison between elastic and rigid bodies
In this procedure, a long-term stress history is required for fatigue damage assessment. This can require excessive CPU time if the ship hull is modeled as an elastic body. Additionally, the bow area of an icebreaker is designed in such a way that local stiffness is very high, comparable to a rigid stiffness. Therefore, the bow of ship is set as a rigid body in the present calculation example. The fatigue stress is subsequently predicted by beam theory. To verify the stress calculated by beam theory, a short-term structural analysis for an elastic model of the ship hull is carried out in the present Appendix.
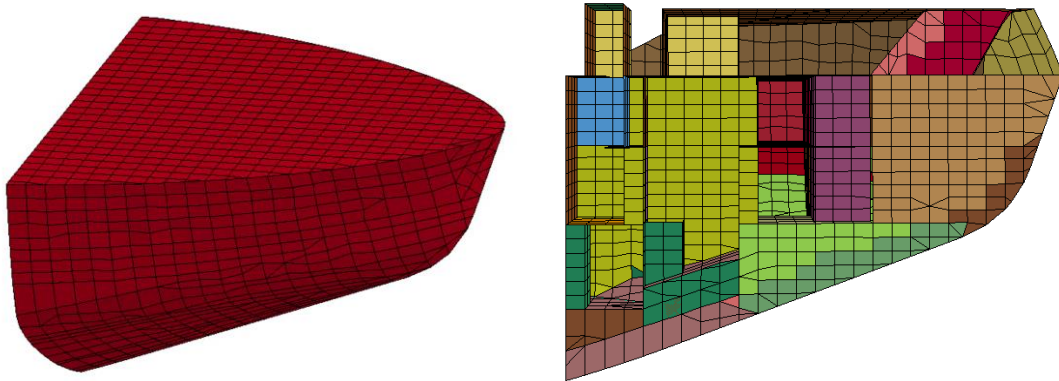

(a) Rigid ship hull model   (b) Elastic ship hull model
Fig. D1 Structural details of the ship hull

For the rigid ship model, only the outer shell (Fig. D1(a)) is built, as the structural details of the rigid hull do not affect the simulated results. The structural details of the elastic hull model can be found in Fig. D1 (b). Unlike the finite element (FE) model for the rigid hull, the elastic ship model contains more beams and stiffeners, which can provide structural stiffness. Most of the FE parameters and numerical settings of the elastic hull model are consistent with those of the rigid model, such as boundary conditions, contact model, and ice material model. The only different numerical settings between the two models are the steel material model and the damping control. For the elastic model, an elastic modulus of 206 GPa is employed. Furthermore, the *DAMPING_PART_STIFFNESS keyword is also applied for the elastic model [18].
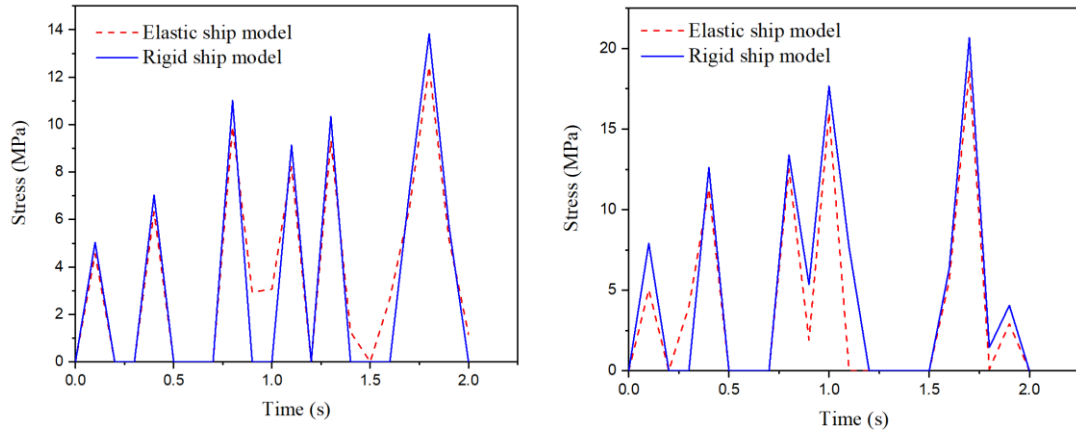
(a) Stress history for the 1.0-m thickness ice condition

(b) Stress history for the 1.5-m thickness ice condition

Fig. D2 Stress histories for different ship models

Fig. D2 presents the comparison of stress histories between the rigid and elastic hull models. The stress peaks for the rigid model are somewhat higher than those for the elastic model. The effect of the hull model properties on the fatigue damage is also considered by Eq. (D1).

$$K_e = D_e / D_r \tag{D1}$$

where

K_e is the ratio of D_e and D_r,

D_e is the fatigue damage for the elastic hull model, and

D_r is the fatigue damage for the rigid hull model.

Table D1 The effect of hull model properties on fatigue damage

Thickness of level ice	Fatigue damage of elastic body, D_e	Fatigue damage of rigid body, D_r	Ratio ($K_e = D_e / D_r$)
1.0 m	2.3064e-8	2.883e-8	0.8
1.5 m	1.139e-8	1.479e-7	0.77

The results of Eq. (D1) are presented in Table D1, and it can be seen that the values of K_e are 0.8 and 0.77 for the 1.0-m-thick and 1.5-m-thick ice conditions, respectively. Therefore, the fatigue damage assessed based on the rigid hull model is approximately 20% higher than that for the elastic hull model. To consider the effect of ship properties on fatigue damage, the modified fatigue damage estimate can be expressed as:

$$D_e = K_e \times D = K_e \frac{N_t}{C} \int_0^{S_{\max}} S^m f_s(S)\,\mathrm{d}S \qquad (D2)$$

References

[1] Postnote. Arctic Changes. London: Parliamentary Office of Science and Technology; 2009. p. 1-4.

[2] Chai W, Leira BJ, Naess A. Short-term extreme ice loads prediction and fatigue damage evaluation for an icebreaker. Ships and Offshore Structures. 2018;13:127-37.

[3] An W-S, Lee T-K, Hwang M-R. Calculation of Fatigue Life of Bow Frame of ARAON Considering Navigating in Ice and Open Waters. Journal of Ocean Engineering and Technology. 2018;32:458-65.

[4] Register Ls. Ship Right Design and Construction, Fatigue Induced by Ice Loading. London: Lloyd's Register Marine Business Stream; 2011.

[5] Suyuthi A, Leira BJ, Riska K. Fatigue damage of ship hulls due to local ice-induced stresses. Appl Ocean Res. 2013;42:87-104.

[6] Han Y, Sawamura J. Calculation of Ship Hull Fatigue Damage Caused by Local Ice Loads in Ridged Ice Fields. The 28th International Ocean and Polar Engineering Conference. Sapporo, Japan: International Society of Offshore and Polar Engineers; 2018. p. 8.

[7] Kim J-H, Kim Y. Numerical simulation on the ice-induced fatigue damage of ship structural members in broken ice fields. Mar struct. 2019;66:83-105.

[8] Srivatsan TS, Imam MA, Srinivasan R. Fatigue of Materials: Cambridge University Press; 1991.

[9] Suominen M, Kujala P, Romanoff J, Remes H. Influence of load length on short-term ice load statistics in full-scale. Mar struct. 2017;52:153-72.

[10] Kotilainen M, Vanhatalo J, Suominen M, Kujala P. Predicting ice-induced load amplitudes on ship bow conditional on ice thickness and ship speed in the Baltic Sea. Cold Reg Sci Technol. 2017;135:116-26.

[11] Ranta J, Polojärvi A, Tuhkuri J. The statistical analysis of peak ice loads in a simulated ice-structure interaction process. Cold Reg Sci Technol. 2017;133:46-55.

[12] Mathworks. MATLAB help documentation: Mathworks; 2019.

[13] Gaidai Oleg SG, Naess Arvid. Extreme Value Statistics of Large Container Ship Roll. SNAME-JSR-2014-58-2-106. 2016;60:92-100.

[14] Naess A, Gaidai O. Estimation of extreme values from sampled time series. Struct Saf. 2009;31:325-34.

[15] Zhang S, Bridges R, Tong J. Fatigue Design Assessment of Ship Structures Induced By Ice Loading-An Introduction to the ShipRight FDA ICE Procedure. The Twenty-first International Offshore and Polar Engineering Conference. Maui, Hawaii, USA: International Society of Offshore and Polar Engineers; 2011. p. 5.

[16] CCS. Rules and regulations for the construction and classification of sea-going steel ships. 82018.

[17] Hallquist JO. LS-DYNA Keyword User's Manual: Livermore Software Technology Corportation (LSTC); 2018.

[18] Hallquist JO. LS-DYNA Keyword User′s Manual (971/R5). California: Livermore Software Technology Corporation, Inc; 2010.

[19] Sazidy M, Daley C, Colbourne B, Wang J. Effect of Ship Speed on Level Ice Edge Breaking. ASME 2014 33rd International Conference on Ocean, Offshore and Arctic Engineering2014.

[20] Timco GW, Weeks WF. A review of the engineering properties of sea ice. Cold Reg Sci Technol. 2010;60:107-29.

[21] Ehlers S, Kujala P. Optimization-based material parameter identification for the numerical simulation of sea ice in four-point bending. Proceedings of the Institution of Mechanical Engineers, Part M: Journal of Engineering for the Maritime Environment. 2013;228:70-80.

[22] Timco GW, Frederking RMW. Compressive strength of sea ice sheets. Cold Reg Sci Technol. 1990;17:227-40.

[23] Timco GW, Frederking RMW. Seasonal Compressive Strength of Beaufort Sea Ice Sheets. Berlin, Heidelberg: Springer Berlin Heidelberg; 1991. p. 267-82.

[24] Timco GW, O.'Brien S. Flexural strength equation for sea ice. Cold Reg Sci Technol. 1994;22:285-98.

[25] Executive TM. China Launches Icebreaker Xuelong 2. 2018.

[26] Suyuthi A, Leira BJ, Riska K. Statistics of local ice load peaks on ship hulls. Struct Saf. 2013;40:1-10.

[27] Lubbad R, Løset S. A numerical model for real-time simulation of ship–ice interaction. Cold Reg Sci Technol. 2011;65:111-27.

[28] Shi W, Tan X, Gao Z, Moan T. Numerical study of ice-induced loads and responses

of a monopile-type offshore wind turbine in parked and operating conditions. Cold Reg Sci Technol. 2016;123:121-39.

[29] Carlos GS, Yordan G. Ships and Offshore Structures XIX. In: Carlos Guedes Soares, Garbatov Y, editors. International Ship and Offshore Structures Congress. Cascais: CRC Press/Balkema; 2015. p. 362-3.

[30] Alvaro A AO. Fundamental Aspects of Fatigue of Steel in Arctic Applications. Alvaro A, Akselsen OM. Busan2014. p. 247-54.

[31] Ellis B, Brigham L. Arctic Marine Shipping Assessment 2009 Report. Arctic Marine Shipping Assessment (ASMA); 2009.

[32] ASTM. Standard practice for conducting constant amplitude axial fatigue tests of metallic materials. The United States2015.

[33] Zhao W, Feng G, Liu W, Ren H. Research on Fatigue Properties of Typical Welded Joints of DH36 Steel at −60 °C. Applied Sciences. 2020;10:3742.

[34] DNV-GL. Fatigue assessment of ship structures. DNV GL; 2015.

[35] Pernas-Sánchez J, Pedroche DA, Varas D, López-Puente J, Zaera R. Numerical modeling of ice behavior under high velocity impacts. Int J Solids Struct. 2012;49:1919-27.

[36] Dempsey JP, Shen HH. IUTAM Symposium on Scaling Laws in Ice Mechanics and Ice Dynamics. 1 ed: Springer Netherlands; 2001.

[37] Iyer SH, Masterson DM. Field strength of multi- year ice using thin-walled fiat jacks. Ninth Interna- tional Conference on Port and Ocean Engineering Under Arctic Conditions. Fairbanks: University of Alaska; 1987.

[38] Hallquist JO. LS-DYNA theory manual: Livermore Software Technology Corportation (LSTC); 2006.

[39] Zingoni A. Advances in Engineering Materials, Structures and Systems: Innovations, Mechanics and Applications: CRC Press; 2019.